Journal of Medicinal Chemistry

Article

Discovery of 3-(5'-Substituted)-benzimidazole-5-(1-(3,5-dichloropyridin-4-yl)ethoxy)-1*H*-indazoles as Potent Fibroblast Growth Factor Receptor Inhibitors: Design, Synthesis and Biological Evaluation

Wei Yan, Xinyi Wang, Yang Dai, Bin Zhao, Xinying Yang, Jun Fan, Yinglei Gao, Fanwang Meng, Yuming Wang, Cheng Luo, Jing Ai, Mei-Yu Geng, and Wenhu Duan

J. Med. Chem., **Just Accepted Manuscript** • DOI: 10.1021/acs.jmedchem.6b00056 • Publication Date (Web): 27 Jun 2016

ACS Publications

Journal of Medicinal Chemistry is published by the American Chemical Society. 1155 Sixteenth Street N.W., Washington, DC 20036

Discovery of 3-(5'-Substituted)-benzimidazole-5-(1-(3,5-dichloropyridin-4-yl)ethoxy)-1*H*-indazoles as Potent Fibroblast Growth Factor Receptor Inhibitors: Design, Synthesis and Biological Evaluation

Wei Yan,[1,#] Xinyi Wang,[2,6,#] Yang Dai,[2] Bin Zhao,[3] Xinying Yang,[2] Jun Fan,[3] Yinglei Gao,[2] Fanwang Meng,[4,5] Yuming Wang,[3] Cheng Luo,[5] Jing Ai,[2,] Meiyu Geng,[2,*] and Wenhu Duan[1,3,*]*

[1]School of Pharmacy, East China University of Science & Technology, 130 Mei Long Road, Shanghai 200237, P.R. China

[2]Division of Anti-tumor Pharmacology, State Key Laboratory of Drug Research, Shanghai Institute of Materia Medica, Chinese Academy of Sciences, 555 Zu Chong Zhi Road, Shanghai 201203, P.R. China

[3]Department of Medicinal Chemistry, Shanghai Institute of Materia Medica, Chinese Academy of Sciences, 555 Zu Chong Zhi Road, Shanghai 201203, P.R. China

[4]Department of Chemistry, College of Sciences, Shanghai University, 99 Shang Da Road, Shanghai 200444, P.R. China

[5]Drug Discovery & Design Center, State Key Laboratory of Drug Research, Shanghai Institute of Materia Medica, Chinese Academy of Sciences, 555 Zu Chong Zhi Road, Shanghai 201203, P.R. China

[6]University of Chinese Academy of Sciences, Beijing, 100049, P.R. China

ABSTRACT

Fibroblast growth factor receptor (FGFR) represents an attractive oncology target for cancer therapy in view of its critical role in promoting cancer formation and progression, as well as causing resistance to approved therapies. In this paper, we describe the identification of the potent pan-FGFR inhibitor (*R*)-**21c** (FGFR1–4 IC_{50} values of 0.9, 2.0, 2.0, and 6.1 nM, respectively). Compound (*R*)-**21c** exhibited excellent *in vitro* inhibitory activity against a panel of FGFR-amplified cell lines. Western blot analysis demonstrated that (*R*)-**21c** suppressed FGF/FGFR and downstream signaling pathways at nanomolar concentrations. Moreover, (*R*)-**21c** provided nearly complete inhibition of tumor growth (96.9% TGI) in NCI-H1581 (FGFR1-amplified) xenograft mice model at the dose of 10 mg/kg/qd via oral administration.

INTRODUCTION

Fibroblast growth factor receptors (FGFRs) are a family of four receptor tyrosine kinases (RTKs), and each of the four FGFRs (FGFR1–4) consists of three extracellular immunoglobulin domains, a single transmembrane domain, and a cytoplasmic tyrosine kinase domain.[1] Upon binding to fibroblast growth factors, the receptor undergoes dimerization and autophosphorylation of tyrosine residues on cytoplasmic tail, resulting in activation of downstream signaling including MEK-ERK, PLCγ, and PI3K-Akt. Physiologically, FGFR pathway plays important roles in embryogenesis, tissue repair and wound healing.[2] FGFR is an oncogenic driver of a broad panel of malignant solid tumors: FGFR1 amplification is identified in about 20% of squamous non-small cell lung carcinoma and about 10% of hormone

receptor-positive breast cancers; FGFR2 is also amplified in about 10% of gastric cancer and 4% of triple-negative breast cancers; mutations of FGFR3 are found in about half of bladder cancers which are strongly related to low-grade tumors; activating mutations of FGFR4 (affecting the kinase domain) are found in 6% to 8% of patients with rhabdomyosarcoma, and overexpression of FGFR4 was found in 50% of hepatocellular carcinomas.[3-8] Moreover, aberrant FGFR activation has been associated with poor prognosis and metastatic progression. In addition, over-activation of FGFR signaling is responsible for *de novo* and acquired resistance to anticancer therapy.[9-11] Therefore, the blockade of FGF/FGFR signaling is considered as an attractive approach for the treatment of cancers.

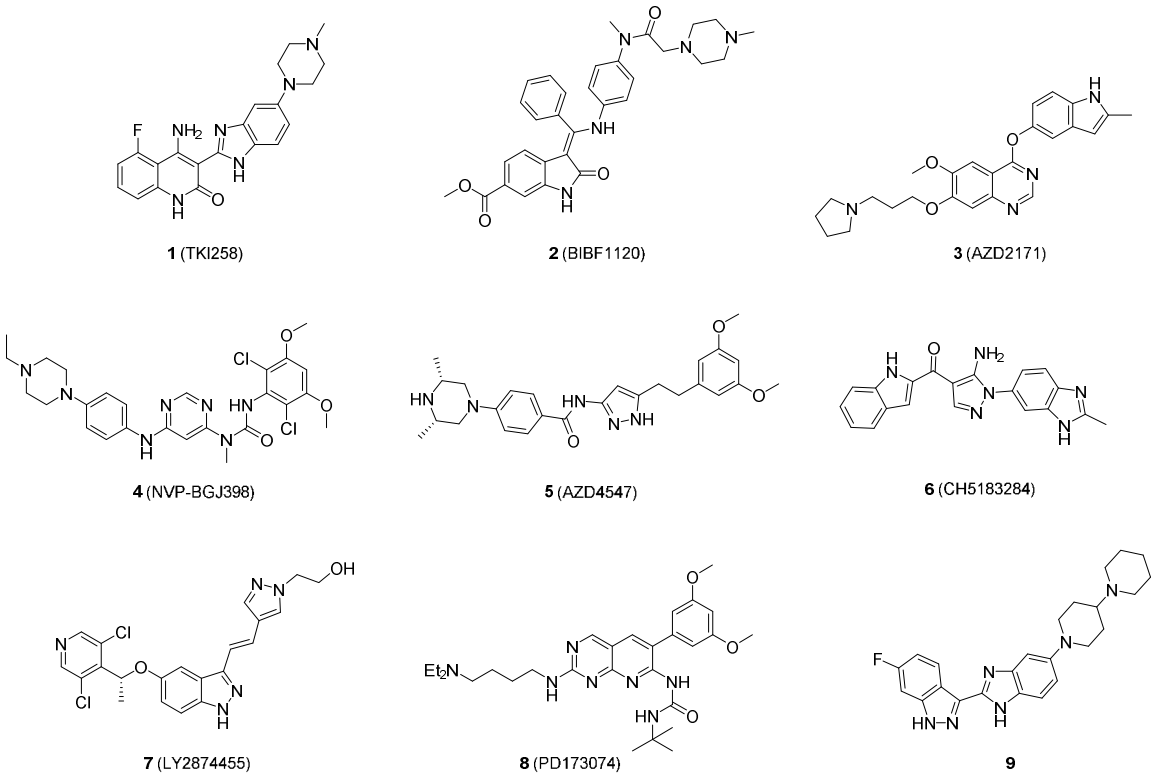

Figure 1. Structures of representative FGFR inhibitors.

The early examples of FGFR inhibitors were non-selective. Owing to the high degree of homology of FGFRs with VEGFRs (vascular endothelia growth factor receptors), many compounds developed as FGFR inhibitors also inhibit VEGFR family members at similar potencies, such as **1** (TKI258),[12] **2**

(BIBF-1120),[13] and **3** (AZD2171)[14] (Figure 1). Although therapies based on inhibiting VEGF/VEGFR signaling pathway have been approved for the treatment of cancers, e.g. **10** (sunitinib),[15] **11** (sorafenib),[16] **12** (pazopanib),[17] and **13** (vandetanib)[18] (Figure 2), undesired side effects such as hypertension and bleeding have been reported.[19-21] Recently, medicinal chemists tend to develop more selective FGFR inhibitors, and several orally available FGFR selective inhibitors have been reported to enter clinical trials, for example, **4** (NVP-BGJ398),[22] **5** (AZD4547),[23] **6** (CH5183284),[24] and **7** (LY2874455)[25] (Figure 1). The 3,5-dimethoxy-phenyl moiety of **4** and **5** occupies the same hydrophobic pocket and forms a hydrogen bond with Asp641, which is identified by **8** (PD173074) to contribute to their selectivity for FGFR1;[26-27] similar interactions are also observed between **6** and FGFR1.[24] Therefore, it is possible that a common single mutation would confer resistance to these inhibitors, which is classified as a category of genetic alteration contributed to the resistance of FGFR inhibitors besides other categories of compensatory pathway activation and epithelial-to-mesenchymal transition, as revealed by limited studies.[24, 28-30]

As illustrated in the binding model of **7** in the ATP binding site of FGFR3,[25] the indazole core binds in the ATP binding pocket and forms two hydrogen bonds with the carbonyl of Glu230 and the NH of Ala232; the vinyl pyrazole fragment extends toward solvent, making important hydrophobic interactions.

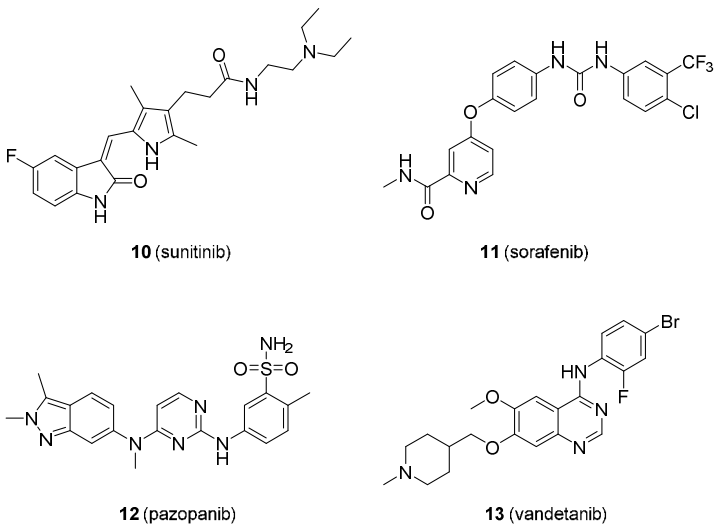

Figure 2. Structures of representative approved VEGFR2 inhibitors.

Additionally, a hydrogen bond between the pyridyl nitrogen and Asn236 in hydrophobic pocket is observed; this additional hydrogen bond increases FGFR binding affinity. We envisioned that the interaction between the pyridine fragment and the hydrophobic pocket might overcome the resistance of the former three FGFR selective inhibitors (**4**, **5**, and **6**) caused by the single mutation as discussed above.

McBride *et al*. reported compound **9** as a dual FGFR1/VEGFR2 inhibitor (Figure 1);[31] this compound showed moderate *in vitro* and *in vivo* antitumor efficiency. To understand the ligand-protein interactions, we developed a binding model of compound **9** in the ATP binding site of FGFR1 with a known crystal structure of the FGFR1 kinase domain (PDB ID: 3WJ6).[24] As shown in Figure 3, compound **9** binds to the hinge region of the kinase and forms two hydrogen bonds with the carbonyl of Glu562 and the NH of Ala564; an additional hydrogen bond occurs between the carbonyl of Ala564 and N(1)-H of benzimidazole moiety; the benzimidazole moiety extends from the indazole 3-position toward solvent exposed region. In view of the high degree of homology of FGFR1 with FGFR3, it was reasonable to assume that **7** and **9** had similar binding patterns with FGFR in the hinge region and the

solvent exposed region. In view of the importance of the interactions between the pyridine fragment and the surrounded hydrophobic pocket, we envisioned that the introduction of a pyridylalkoxy moiety to the indazole benzimidazole scaffold might form a novel series of FGFR inhibitors with improved potency and selectivity. To test our hypothesis, we designed and synthesized a series of novel 3-benzimidazole-5-pyridylalkoxy-1*H*-indazole derivatives (Figure 4), and these new derivatives displayed excellent *in vitro* and *in vivo* antitumor activities. Herein, we report the detailed synthesis and biological evaluation of these compounds.

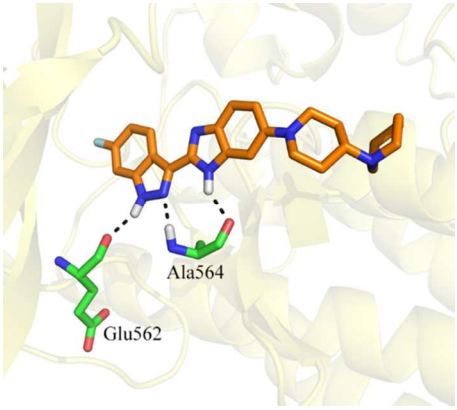

Figure 3. Proposed binding mode of compound **9** to FGFR1 kinase domain. The atoms of compound **9** are colored as follows: carbon orange, oxygen red, nitrogen blue, fluorine light blue, and hydrogen white. The docked protein structure of FGFR1 is shown in the cartoon and key residues are colored as follows: carbon green, oxygen red, nitrogen blue, and hydrogen white. The hydrogen bonds are colored in black.

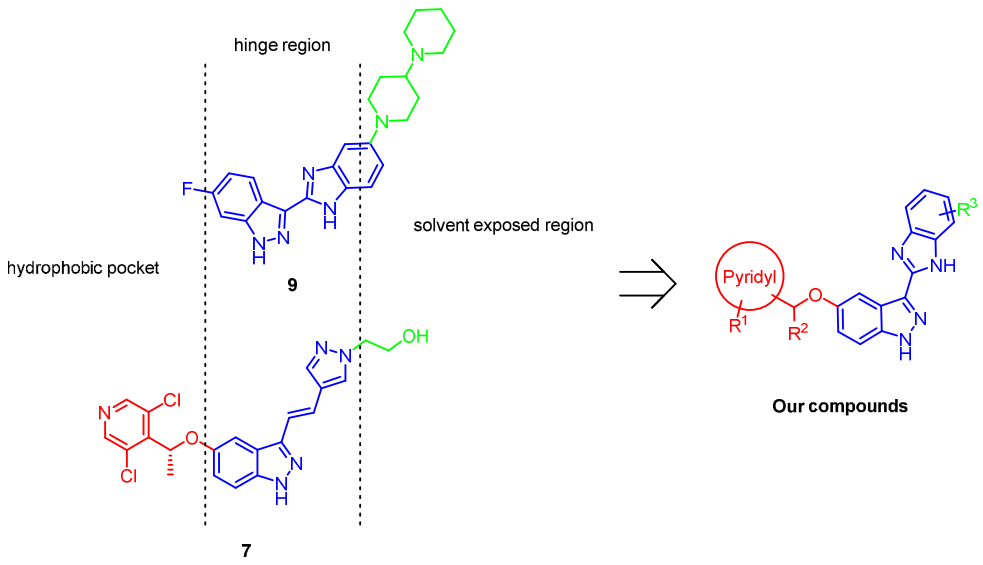

Figure 4. Design of our compounds.

RESULTS AND DISCUSSION

Lead Optimization and Identification of Compound (*R*)-21c.

To evaluate the aforementioned hypothesis, we prepared compound **14a** as the proof-of-concept compound, which possessed moderate enzymatic activity (Table 1). In order to get a putative binding mode, a molecular docking simulation was performed. As depicted in Figure 5, **14a** maintained all the critical interactions observed in compounds **7** and **9**: the indazole core was anchored to the hinge region of kinase domain via two highly conserved hydrogen bonds with the carbonyl of Glu562 (1.8 Å) and the amino group of Ala564 (2.1 Å); an additional hydrogen bond occurred between the carbonyl of Ala564 and N(1)-H of benzimidazole moiety (2.3 Å); a hydrogen bond between pyridyl nitrogen atom and amino group of Asn568 (2.3 Å) was formed as expected, which reinforced this binding conformation.

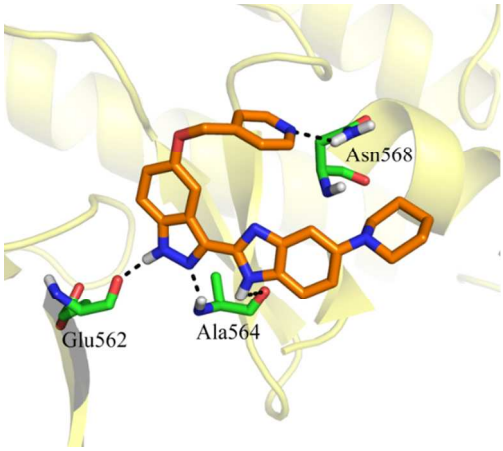

Figure 5. Proposed binding mode of compound **14a** to FGFR1 kinase domain. The atoms of compound **14a** are colored as follows: carbon orange, oxygen red, nitrogen blue, and hydrogen white. The docked protein structure of FGFR1 is shown in the cartoon and key residues are colored as follows: carbon green, oxygen red, nitrogen blue, and hydrogen white. The hydrogen bonds are colored in black.

For initial structure-activity relationship exploration, **14a** served as a benchmark to analyze both enzymatic and cellular potency contributions from different pyridine ring substitution patterns, and compound **5** was used as the positive control. Despite its moderate potency against FGFR1, **14a** displayed a weak inhibitory effect in NCI-H1581 proliferation assay (IC_{50} of 5016.9 nM). Incorporation of a chlorine atom at the 3-position of the pyridine ring provided **14b**, which displayed measurable increases in potencies; when an additional chlorine was introduced to the 5-position, the 3,5-dichloro derivative **14c** exhibited a 31-fold increase compared to **14a** in cellular potency with an IC_{50} of 158.7 nM; further introduction of an α-methyl into **14c** afforded **15a**, which demonstrated a further eleven-fold enhancement of cellular potency compared to **14c** (IC_{50} of 14.1 nM) and 7- and 54-fold increases compared with

Table 1. Structure-activity Relationship of Substitutions on Racemic 5-Pyridylalkoxy Group

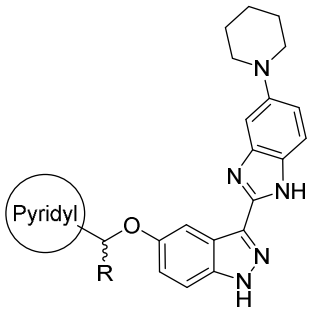

Compound	Pyridyl	R	FGFR1 (IC_{50}, nM)[a]	NCI-H1581 Cell (IC_{50}, nM)[a]
14a	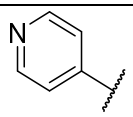	H	20.8 ± 2.3	5016.9 ± 450.0
14b	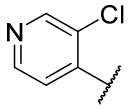	H	13.6 ± 1.7	3071.1 ± 252.2
14c	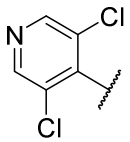	H	6.6 ± 0.8	158.7 ± 3.0
14d	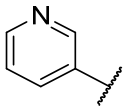	H	1.7 ± 0.1	1859.1 ± 156.4
14e	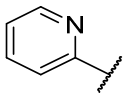	H	4.1 ± 0.8	1232.4 ± 121.7
15a	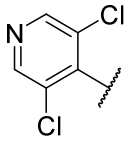	Me	2.7 ± 0.8	14.1 ± 2.1
15b	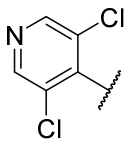	Et	5.7 ± 2.3	380.1 ± 21.8

15c	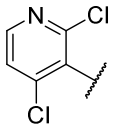	Me	22.4 ± 4.2	30.8 ± 4.2
9	–	–	20.3 ± 1.3	749.1 ± 47.2
7	–	–	0.3 ± 0.1	< 0.5
5	–	–	0.6 ± 0.2	92.1 ± 2.8

[a] Values are the mean ± SD of two independent assays.

compound **9** in enzymatic and cellular potencies, respectively. The increases in potency of compounds **14b**, **14c**, and **15a** might be explained by the increased lipophilicity by inclusion of the chlorine atom and the α-methyl.[32] The ethyl analogue **15b** retained enzymatic potency but turned out to be 27-fold less active than **15a** in the NCI-H1581 proliferation assay. Next, we assessed the importance of the position of the pyridine nitrogen by synthesizing compounds **14d** and **14e**. Interestingly, when pyridine nitrogen was moved to the 2-position, the resulting compound **14d** was more potent than the 1- or 3-pyridyl analogues (**14a** and **14e,** respectively). These results implied that the 2-pyridyl isomer interacted in a more favorable manner with the protein; however, when 3,5-dichloro and α-methyl were introduced to **14d**, the resulting compound **15c** was eight- and two-fold less active than **15a** in enzymatic and cellular potencies, respectively. Therefore, **15a** with the 3,5-dichloro and α-methyl substitution pattern was chosen as the compound for further optimization.

Table 2. Structure-activity Relationship of 3-Heterocycle Substitutions on Racemic 5-(1-(3,5-Dichloropyridin-4-yl)ethoxy)-1*H*-indazole

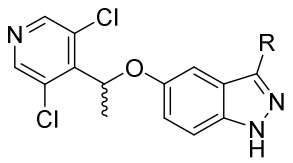

Compound	R	FGFR1	NCI-H1581 Cell

		(IC_{50}, nM)[a]	(IC_{50}, nM)[a]
16a	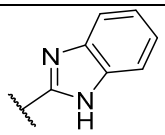	1.8 ± 0.1	402.7 ± 13.6
16b	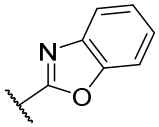	5.1 ± 0.6	3035.7 ± 593.3
16c	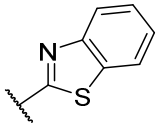	228.2 ± 27.1	> 10000
17	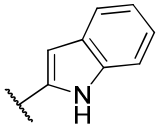	2.4 ± 0.6	817.2 ± 13.5

[a] Values are the mean ± SD of two independent assays.

We next turned our attention to the benzimidazole moiety by replacing it with three other heterocyclic bioisosteres. The substituent at the 5'-position was removed for rapid evaluation of the impact of this replacement (Table 2), which led to compound **16a** with modest cellular potency. Compared with **16a**, benzoxazole analogue **16b** displayed three- and eight-fold decreases in enzymatic and cellular potencies, respectively. The decrease in potency of **16b** could be explained by the absence of the hydrogen bond formed between benzimidazole NH and Ala564. Replacement of the benzimidazole moiety by benzothiazole completely eroded the cellular activity (**16c**). Indole analogue **17** retained FGFR activity but was two-fold less active than **16a** in NCI-H1581 proliferation assay. These results revealed that the benzimidazole moiety was optimal for FGFR activity.

Table 3. Structure-activity Relationship of Substitutions on Benzimidazole

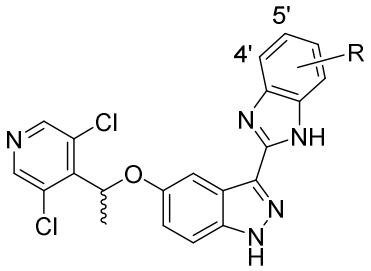

Compound	4’	5’	FGFR1 (IC_{50}, nM)[a]	NCI-H1581 Cell (IC_{50}, nM)[a]
16a	H	H	1.8 ± 0.1	402.7 ± 13.6
18a	Me	H	16.2 ± 2.4	> 10000
18b		H	> 1000	NT[b]
19a	H	F	2.1 ± 0.4	582.3 ± 66.4
19b	H	Me	2.0 ± 0.1	922.3 ± 94.6
19c	H	OMe	2.8 ± 0.6	315.3 ± 11.7
19d	H		2.1 ± 0.2	5.5 ± 2.4
20	H	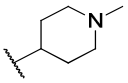	1.0 ± 0.1	1.6 ± 1.2
21a	H	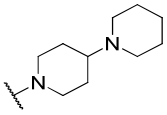	0.8 ± 0.1	10.3 ± 0.65
21b	H	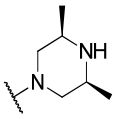	1.4 ± 0.1	1.9 ± 0.5
21c	H	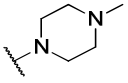	1.0 ± 0.2	1.0 ± 0.2

21d	H	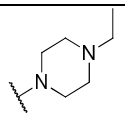	3.6 ± 0.9	5.9 ± 2.9
21e	H	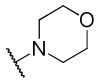	0.2 ± 0.0	2.2 ± 0.5
21f	H	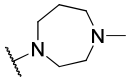	7.6 ± 1.4	8.1 ± 1.1
19e	H	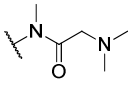	0.4 ± 0.2	0.8 ± 0.1
21g	H	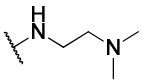	0.3 ± 0.1	1.1 ± 0.2
21h	H	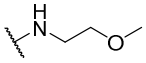	0.6 ± 0.1	1.2 ± 0.6
22	H	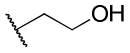	1.5 ± 0.1	3.3 ± 1.1

[a]Values are the mean ± SD of two independent assays.

[b]Not tested.

Finally, systematic structural optimization of benzimidazole of **16a** revealed that substituents on the benzimidazole dramatically impacted FGFR inhibition. As summarized in Table 3, the 4'-methyl analogue **18a** showed a nine-fold drop in enzymatic potency compared with **16a** and had a cellular IC_{50} greater than 10000 nM; moreover, the attachment of a 4'-piperidyl group to the benzimidazole moiety (**18b**) resulted in a significant loss of activity (FGFR1 kinase IC_{50} greater than 1000 nM). These results revealed that substitution at 4'-position of the benzimidazole moiety was not tolerable. On the contrary, inclusion of substituents at the 5'-position of the benzimidazole had favorable impacts: derivatives bearing hydrophobic groups (such as fluoro, methyl, and methoxyl) retained enzymatic and cellular potencies (compounds **19a**–**c**); moreover, when the hydrophilic methylamino was attached to the 5'-position of benzimidazole, the resulting derivative **19d** exhibited a cellular potency with an IC_{50} less

than 10 nM in the NCI-H1581 proliferation assay. Therefore, we introduced a number of amines and alcohol to the 5'-position of the benzimidazole moiety. In general, six-membered ring analogues (**20** and **21b**–**e**) had comparable potencies; but 1-ethylpiperazine analogue **21d** was nearly four- and six-fold less active than methyl analogue **21c** in enzymatic and cellular potencies, respectively; the piperidinylpiperidine analogue **21a** had a FGFR1 IC_{50} of 0.8 nM, but suffered a twelve-fold enzyme-to-cell shift, resulting in a cellular IC_{50} of 10 nM; the homopiperazine analogue **21f** was eight-fold less active compared with **21c**. The relatively low potency of **21a**, **21d**, and **21f** indicated that the larger ring substitution was less tolerable. Compounds bearing chain substituents (**19e**, **21g**–**h**, and **22**) also turned out to be very potent, and they had comparable potencies to the cyclic amines. As discussed above, a range of functional groups were tolerated at the 5'-position of the benzimidazole moiety, potentially owing to this region extending out of the kinase domain of FGFR1 into a solvent exposed region.

Because of the undesired side-effects caused by inhibiting VEGFR2 signaling pathway, five compounds with excellent enzymatic and cellular potencies were selected to be evaluated for their VEGFR2 kinase inhibition. As listed in Table 4, all tested compounds displayed six- to eight-fold selectivity for FGFR1 over VEGFR2, while compound **9** was nearly equipotent against FGFR1 and VEGFR2. This result

Table 4. FGFR Selectivity of Selected Compounds

Compound	FGFR1 (IC_{50}, nM)[a]	VEGFR2 (IC_{50}, nM)[a]	VEGFR2/FGFR1 ratio
20	1.0 ± 0.1	7.8 ± 1.3	7.8
21b	1.4 ± 0.1	9.0 ± 1.0	6.4
21c	1.0 ± 0.2	8.0 ± 0.5	8.0
19e	0.4 ± 0.2	2.5 ± 0.5	6.2

22	1.5 ± 0.1	12.6 ± 0.9	8.4
9	20.3 ± 1.3	16.4 ± 0.9	0.8
7	0.3 ± 0.1	5.8 ± 0.4	14.5
5	0.6 ± 0.2	27.0 ± 3.4	45.0

[a]Values are the mean ± SD of two independent assays.

revealed that incorporation of 5-(1-(3,5-dichloropyridin-4-yl)ethoxyl fragment at the 5-position of the indazole enhanced FGFR inhibitory activity and selectivity over VEGFR2. On the basis of their enzymatic and cellular inhibitory activities, compounds **21c** and **22** were chosen for further evaluation.

Compounds **21c** and **22** were racemates; the enantiomers of **21c** and **22** were resolved to evaluate the relative FGFR activity. As illustrated in Figure 6, the *R* enantiomers were significantly more potent; the result was also consistent with the specific binding revealed in a docking model of compound (*R*)-**21c** to FGFR1 (Figure 9, *vide infra*).

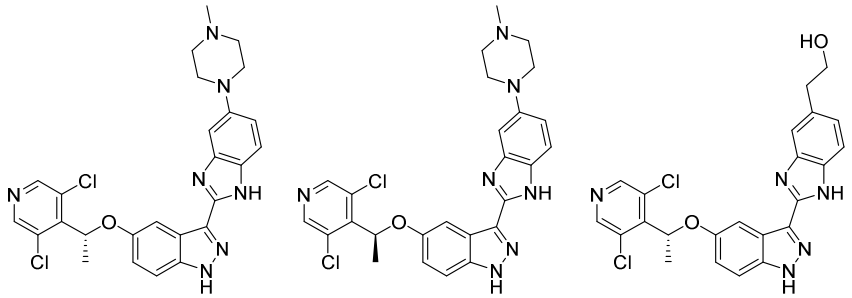

Compound	FGFR1 IC_{50} (nM)	NCI-H1581 IC_{50} (nM)
(*R*)-**21c**	0.9	4.2
(*S*)-**21c**	9.4	129.5
(*R*)-**22**	1.2	1.4
(*S*)-**22**	6.5	>100

Figure 6. Structures and activities of the enantiomers of **21c** and **22**.

Pharmacokinetic Profiles of Compounds (*R*)-21c and (*R*)-22.

Compound (*R*)-**21c** or (*R*)-**22** was administrated to male Sprague-Dawley (SD) rats: either as a 1 mg/kg intravenous or orally by gavage at a 5 mg/kg dose and the relevant pharmacokinetic parameters were summarized in Table 5. Both compounds exhibited moderate and similar plasma clearance (2.0 and 1.7 L/h/kg, respectively) and oral exposed (798.6 and 663.9 ng·h/mL, respectively). Compound (*R*)-**22** had a long half-time (7.3 h) but also had a very large volume of distribution (17.6 L/kg) and relatively low oral bioavailability (22%); while (*R*)-**21c** had a moderate half-time (2.0 h), volume of distribution (5.8 L/kg), and oral bioavailability (33%). Taking all their data into consideration, we selected compound (*R*)-**21c** to further evaluate its *in vitro* and *in vivo* antitumor activities.

Table 5. Pharmacokinetic Profile of (*R*)-**21c** and (*R*)-**22** in Rats[a]

Compound	Dose (mg/kg)	C_{max} (ng/mL)	T_{max} (h)	$T_{1/2}$ (h)	$AUC_{0\rightarrow\infty}$ (ng·h/mL)	CL (L/h/kg)	V_{ss} (L/kg)	*F* (%)
(*R*)-**21c**	1 (*iv*)	300.3	–	2.0	485.3	2.0	5.8	–
	5 (*po*)	97.2	4.0	–	798.6	–	–	33
(*R*)-**22**	1 (*iv*)	735.4	–	7.3	582.3	1.7	17.6	–
	5 (*po*)	195.3	0.8	–	663.9	–	–	22

[a] C_{max}, maximum concentration; T_{max}, time of maximum concentration; $T_{1/2}$, elimination half-life; $AUC_{0\rightarrow\infty}$, area under the plasma concentration time curve; CL, clearance; V_{ss}, volume of distribution; *F*, oral bioavailability.

Kinase Inhibition Profile of (*R*)-21c.

By use of an ELISA-based enzymatic assay, (*R*)-**21c** was distinguished for its high potency against FGFR1 kinase activity. Then we were prompted to investigate its activity against a panel of tyrosine kinases. Compound (*R*)-**21c** showed almost equal potency against FGFR2 and FGFR3, a little weaker against FGFR4, with IC_{50} values of 2.0, 2.0, and 6.1 nM, respectively, indicating (*R*)-**21c** was a pan-

FGFR inhibitor (Table 6). Compared with compound **5** (FGFR4 IC_{50} of 165 nM, literature reported data[23]), (*R*)**-21c** was significantly more potent in inhibiting FGFR4, indicating its potential use for the treatment of FGFR4-driven cancer types, for example, hepatocellular carcinoma (HCC).[8, 33] Furthermore, (*R*)**-21c** was extended to be profiled against a panel of 54 human kinases, including FGFR homologous PDGFR kinase family (PDGFRα, PDGFRβ). Compared to its high potency against FGFR, (*R*)**-21c** exhibited much weaker potency against these tested kinases (IC_{50} >100 nM, or 1000 nM) (Table 6 and Table S1), indicating that (*R*)**-21c** was a selective FGFR inhibitor.

Table 6. Kinase Inhibition Profile of (*R*)-**21c**

Tyrosine kinase[a]	IC_{50} (nM)[b]	Tyrosine kinase[a]	IC_{50} (nM)[b]
FGFR1	0.9 ± 0.2	PDGFRβ	> 1000
FGFR2	2.0 ± 0.5	c-Met	> 100
FGFR3	2.0 ± 0.3	Flt1	> 100
FGFR4	6.1 ± 0.4	Flt3	> 100
VEGFR2	7.5 ± 0.8	RET	> 100
EGFR	> 1000	c-Src	> 100
ErbB2	> 1000	Bcr-Abl	> 100
PDGFRα	781.8 ± 7.6	EPHA2	> 100

[a]EGFR, epidermal growth factor receptor; PDGFR, platelet derived growth factor receptor; c-Met, mesenchymal epithelial transition growth factor; Flt, fms-like tyrosine kinase; RET, rearranged during transfection; c-Src, cellular Src kinase; Bcr-Abl, breakpoint cluster region-abelson; EPHA, erythropoietin-producing hepatocellular carcinoma receptor.

[b]Values are the mean ± SD of three independent assays.

Inhibition on FGFR Signaling of Compound (*R*)-21c

To further evaluate the cellular activity of (*R*)-**21c** targeting FGFR kinase, we analyzed its effects on the phosphorylation of FGFR and its major downstream signaling molecules, PLCγ and Erk. Two representative cancer cell lines with different mechanisms of FGFR activation, FGFR1-fusion protein driven human myeloid leukemia cancer cell line KG-1 and FGFR2-amplified dependent human gastric cancer cell line SNU-16, were chosen. As shown in Figure 7, (*R*)-**21c** significantly inhibited the phosphorylation of FGFR1 in a dose dependent manner in KG1 cells. In line with suppressed FGFR1 phosphorylation, the phosphorylation of PLCγ and Erk, the main downstream molecules of FGFR, was also strongly inhibited. Similar results were observed in (*R*)-**21c** treated SNU-16 cells. These results suggested that (*R*)-**21c** exhibited an effective blockage of FGFRs signaling.

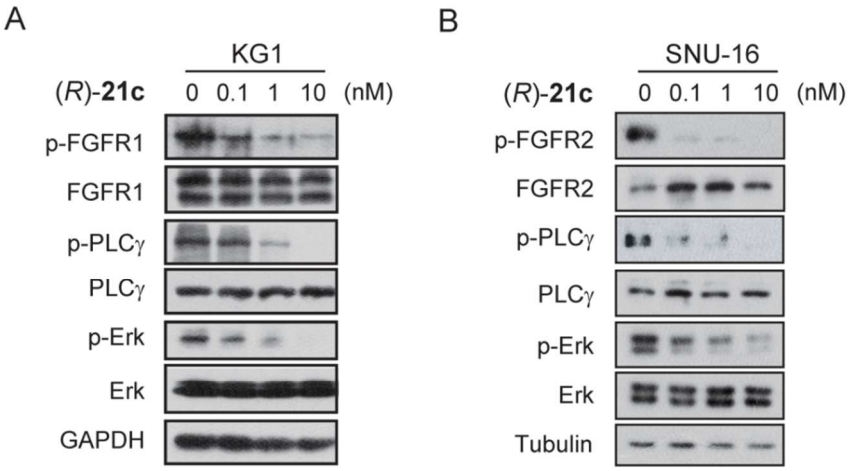

Figure 7. Compound (*R*)-**21c** effectively inhibits the phosphorylation of FGFR and the downstream effectors PLCγ and Erk in KG-1 and SNU-16 cells. KG1 (A) or SNU-16 (B) cells treated with *(R)*-**21c** for 2 h at the indicated concentrations were lysed and subjected to western blot analysis.

Inhibition on FGFR Signaling-driven cancer cell proliferation of (*R*)-21c

Increased FGFR signaling promotes cancer cell proliferation. To elucidate the impact of (*R*)**-21c** on FGFR mediated cancer cell proliferation, four FGFR-driven cancer cell lines harboring the frequently occurring oncogenic forms of FGFRs were chosen: FGFR1 translocated KG1 cells, FGFR1-amplified NCI-H1581 cells, FGFR2-amplified SNU16 cells, FGFR3-amplified RT112 cells. As shown in Table 7, compound (*R*)**-21c** strongly inhibited cell proliferation of KG1, NCI-H1581, SNU16, RT112 cells, with most of the IC_{50} values of less than 0.1 nM, which was much more potent than that of compound **5**, the most advanced pan-FGFR inhibitor in clinical studies.[1] These findings suggested that (*R*)-21c strongly inhibited FGFR-driven cancer cell proliferation via blocking FGFR signaling.

Table 7. Antiproliferative Activity of (*R*)**-21c** on FGFR Addicted Cell Lines

Cell lines	IC_{50} (nM)[a]	
	(*R*)**-21c**	**5**
KG-1	< 0.1	6.4 ± 1.1
NCI-H1581	4.2 ± 2.5	58.8 ± 1.4
SNU16	< 0.1	13.4 ± 0.3
RT112	< 0.1	88.4 ± 10.5

[a]Values are the mean ± SD of three independent assays.

In Vivo Antitumor Activity of Compound (*R*)-21c

To assess the *in vivo* antitumor efficacy of (*R*)**-21c**, NCI-H1581 xenograft mouse model, which is driven by amplification of FGFR1, was used. Compound (*R*)**-21c** was orally administrated once daily at doses of 2 or 10 mg/kg for 21 consecutive days. The results showed that (*R*)**-21c** could suppress tumor

growth in a dose-dependent manner, with the tumor growth inhibition rate (TGI) of 44.5% and 96.9% at the doses of 2 mg/kg and 10 mg/kg, respectively, without significant body loss (Figure 8), indicating (*R*)-**21c** elicited a robust antitumor efficacy in a FGFR-dependent tumor model. Therefore, (*R*)-**21c** was a potential FGFR inhibitor candidate for further drug development.

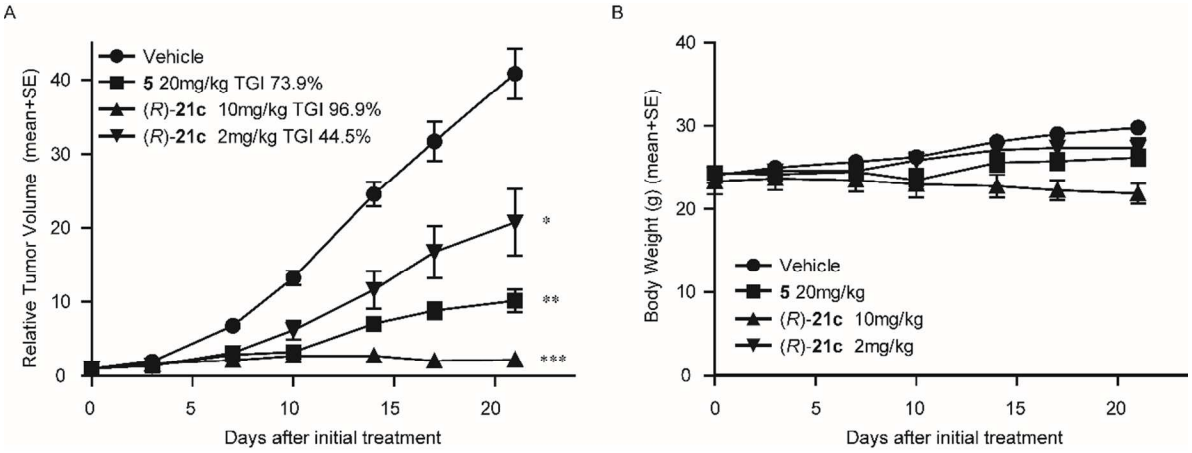

Figure 8. The inhibitory effect of (*R*)-**21c** on tumor growth in NCI-H1581 xenograft model. Compound (R)-21c was administered orally once daily for 21 days. (A) The percentage of tumor growth inhibition values (TGI) was measured on the final day of the study for the drug-treated mice compared with the vehicle control mice: (∗) $P< 0.05$, (∗) $P< 0.01$, (∗) $P< 0.001$, versus vehicle group, using Student's t test. Results are expressed as the mean ± SEM (n = 6 for inhibitor-treated group, n = 12 for vehicle control group). (B) Body weight measurements during the treatment.

Molecular Docking Study of Compound (*R*)-21c to FGFR1

As illustrated in Figure 9, (*R*)-**21c** had a similar binding mode with **14a**: the indazole core was anchored to the hinge region of FGFR1 kinase domain via two highly conserved hydrogen bonds with Glu562 and Ala564; a hydrogen bond between pyridyl nitrogen atom and Asn568 was formed as expected. The α-methyl in the linkage between pyridine ring and the indazole core had a favored steric effect: as indicated in Figure 9C, the *R*-methyl fit in a pocket surrounded by Asp641, Val492, and

Glu485, thus compelling the pyridine ring to form a strong hydrogen bond with Asn568; on the contrary, an *S*-methyl would have an unfavored steric hindrance effect with Val492 which would destabilize the active conformation. The benzimidazole moiety was located in a narrow hydrophobic cleft that was formed by five residues (namely, Leu484, Tyr563, Ala564, Ser565, and Gly567): an additional hydrogen bond occurred between the carbonyl of Ala564 and N(1)-H of benzimidazole moiety that reinforced this binding conformation; the 4'-position of benzimidazole was surrounded by Leu484, Ser565, and Gly567; while the 5'-substitution extended out of this pocket into the solvent exposed region; this binding information explained why 4'-substitution of benzimidazole was not tolerable, but a range of functional groups were tolerated at the 5'-position.

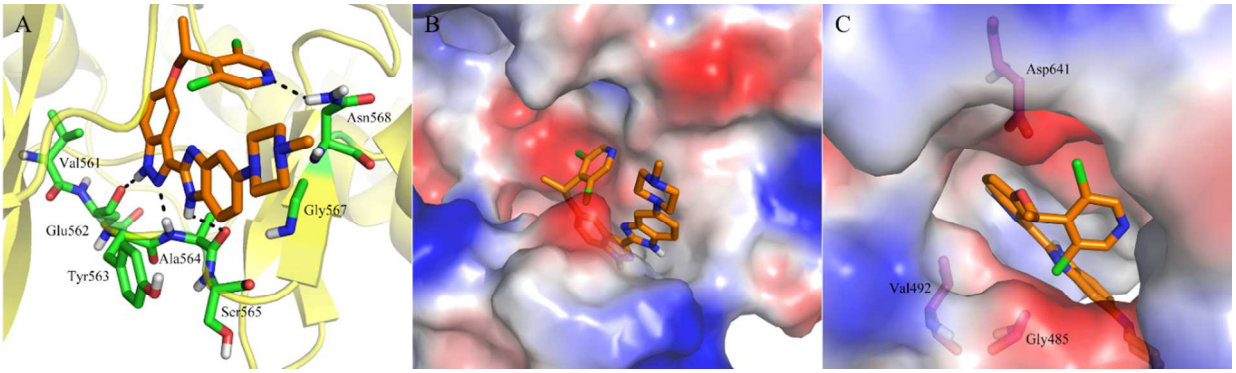

Figure 9. The proposed binding mode of (*R*)-**21c** with FGFR1. (A) The atoms of (*R*)-**21c** are colored as follows: carbon orange, oxygen red, nitrogen blue, chlorine green, and hydrogen white. The docked protein structure of FGFR1 is shown in the cartoon and key residues are colored as follows: carbon green, oxygen red, nitrogen blue, and hydrogen white. The hydrogen bonds are colored in black. (B) The docked protein structure of FGFR1 is shown in surface. The surfaces of Gly485 and Glu486 are omitted for clarity. (C) The *R*-methyl fit in a pocket surrounded by three residues (Asp641, Val492, and Glu485).

CHEMISTRY

Scheme 1[a]

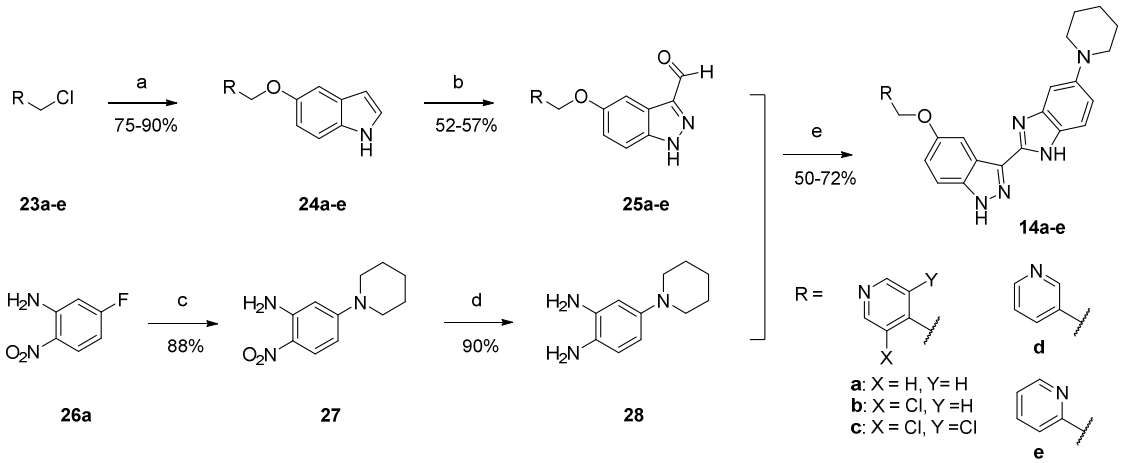

[a]Reagents and conditions: (a) 5-hydroxyindole, Cs_2CO_3, DMF, 70 °C; (b) $NaNO_2$, HCl, H_2O/dioxane, 0 °C to rt; (c) Et_3N, piperidine, NMP, 120 °C; (d) H_2, 10% Pd/C, MeOH, rt; (e) S_8, DMF, 90 °C.

As outlined in Schemes 1–2, benzyl chlorides **23** or methane sulfonates **31** were reacted with 5-hydroxy-1*H*-indole to provide ethers **24** or **32**, which were transformed to 3-carbaldehyde-1*H*-indazoles **25** or **33** by treatment of dilute nitrous acid.[34] Nucleophilic displacement of the C-5 fluorine of **26a** with piperidine afforded **27**. Reduction of **27** with hydrogen afforded diamine **28** which should be protected in argon atmosphere during workup and reacted immediately after workup with aldehydes **25** or **33** to afford compounds **14** and **15**.

Compounds **16a** and **16c** were prepared by analogous methods (Scheme 3); while the stronger oxidant DDQ rather than sulfur was used in the final cyclo-condensation step in the preparation of **16b**. The indole-indazole derivative **17** was synthesized via palladium-catalyzed cross-coupling reaction of iodide **35** and boronic acid **36**; compounds **35** and **36** were prepared according to literature procedures.[35-36]

Scheme 2[a]

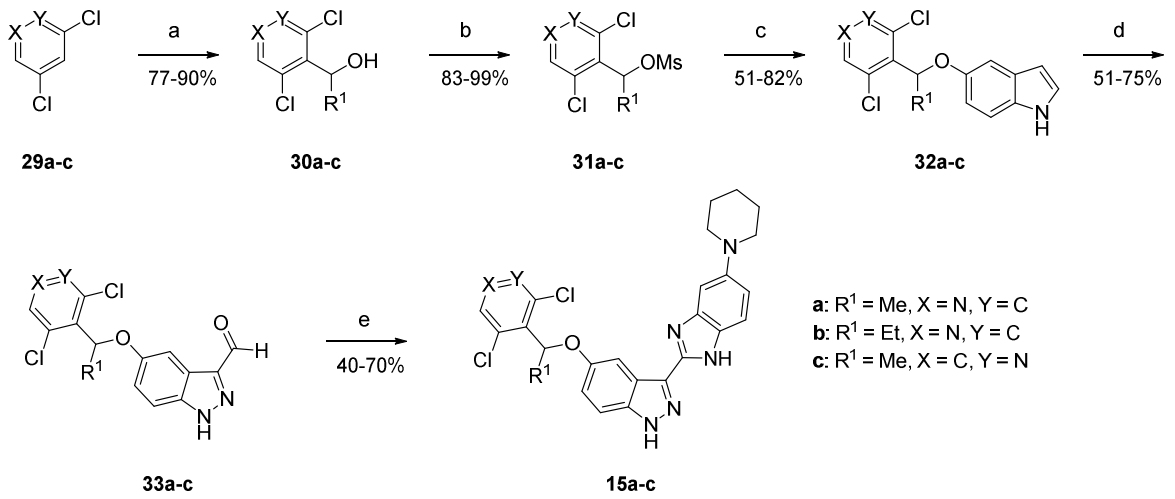

[a]Reagents and conditions: (a) for **30a** and **30c**, LDA, acetaldehyde, THF, −78 °C; for **30b**, LDA, propionaldehyde, THF, −78 °C; (b) MsCl, Et_3N, CH_2Cl_2, 0 °C to rt; (c) 5-hydroxyindole, Cs_2CO_3, DMF, 70 °C; (d) $NaNO_2$, HCl, H_2O/dioxane, 0 °C to rt; (e) **28**, S_8, DMF, 90 °C.

Scheme 3[a]

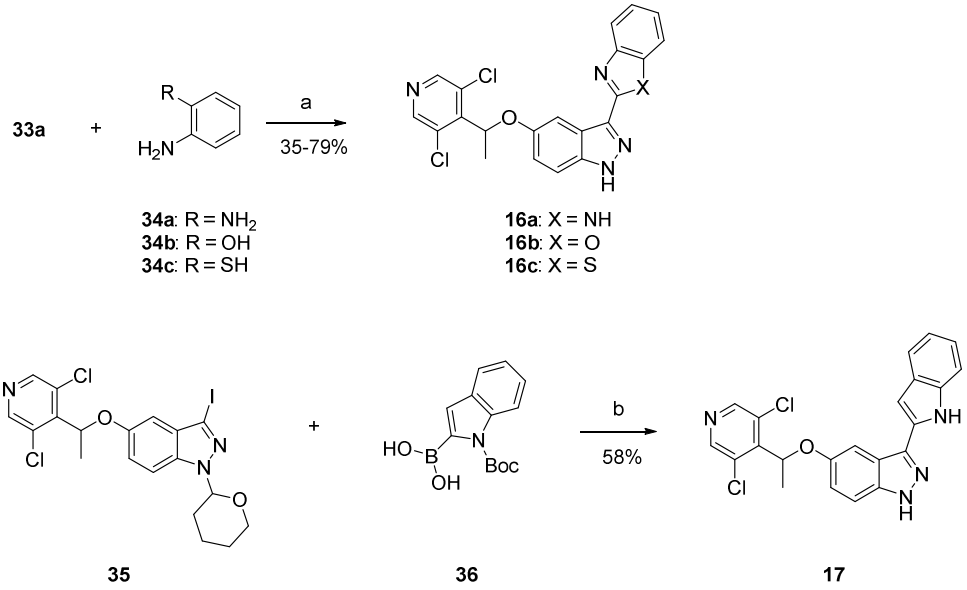

[a]Reagents and conditions: (a) for **16a** and **16c**, S_8, DMF, 90 °C; for **16b**, (i) DMF, 90 °C; (ii) DDQ, $CHCl_3$, reflux; (b) (i) Cs_2CO_3, $Pd(dppf)_2Cl_2$, dioxane, 90 °C; (ii) 4 N HCl in MeOH.

Compounds **18**–**22** were prepared via a similar route (Scheme 4). An array of 2-nitroaniline intermediates (**40**) were prepared starting from **26a** by displacement of fluorine with commercial available amines (**39**). Acylation of amine **19d** with bromoacetyl chloride followed by displacement of

the bromine with dimethylamine furnished amide **19e**. Intermediates **38** and **41** were prepared according to literature procedures.[37-38]

Scheme 4[a]

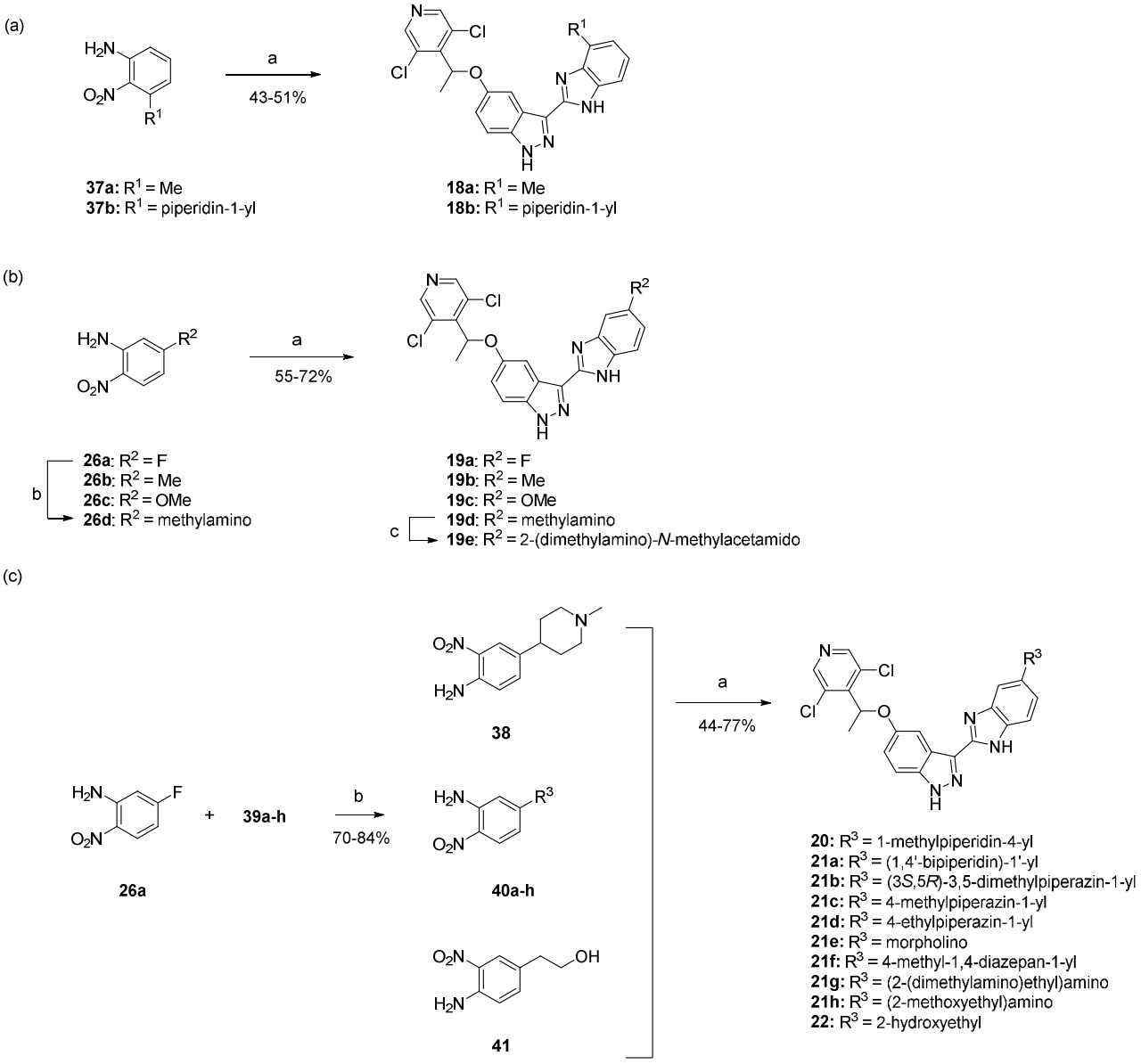

[a]Reagents and conditions: (a) (i) H_2, 10% Pd/C, MeOH, rt; (ii) **33a**, S_8, DMF, 90 °C; (b) for **26d**, methylammonium chloride, DIPEA, NMP, 140 °C; for **40**, DIPEA, NMP, 120 °C; (c) (i) 2-bromoacetyl chloride, CH_2Cl_2, rt; (ii) dimethylamine, THF, rt.

The enantiomers of **21c** and **22** were resolved to evaluate the relative FGFR activities. The racemic alcohol **30a** was reacted with chiral acid **42** via kinetic resolution reaction (twice) to give (*S*)-**30a** with an enantiomeric excess (ee) of 98% (Scheme 5).[39] Mitsunobu reaction of (*S*)-**30a** with acetic acid followed by hydrolysis with sodium hydroxide afforded (*R*)-**30a** in nearly complete configuration inversion (ee 97%). Compound (*R*)-**21c** was prepared starting from (*S*)-**30a** in a similar manner as described for the racemic **21c** (Scheme 6). It was noted that partial racemization was observed in the S_N2 ether formation step, and the ee of (*R*)-**32a** was 89%; the corresponding aldehyde was suspended in ethyl acetate and filtered to generate enantiomerically pure (*R*)-**33a** with an ee of over 99%.

Scheme 5[a]

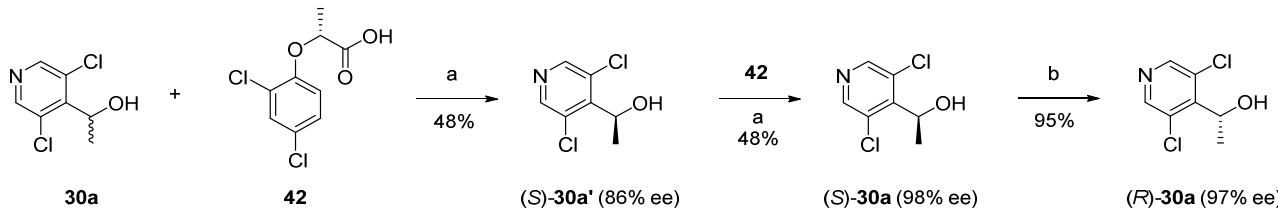

30a **42** (*S*)-**30a'** (86% ee) (*S*)-**30a** (98% ee) (*R*)-**30a** (97% ee)

[a]Reagents and conditions: (a) (i) DCC, 4-DMAP, toluene, 0 °C; (ii) NaOH, H_2O, EtOH, rt; (b) (i) HOAc, DIAD, PPh_3, THF, 0 °C to rt; (ii) NaOH, H_2O, EtOH, rt.

CONCLUSION

In summary, we have developed a series of 3-(5'-substituted)-benzimidazole-5-(1-(3,5-dichloropyridin-4-yl)ethoxy)-1*H*-indazoles as potent FGFR inhibitors. Structural optimization of **14a** led to the identification of (*R*)-**21c**, which had pan-FGFR inhibitory activities against FGFR1–4 (IC_{50} values of 0.9, 2.0, 2.0, and 6.1 nM, respectively) and eight-fold selectivity over VEGFR2. Compared with other FGFR selective inhibitors, (*R*)-**21c** potently inhibited FGFR4, indicating its potential use for the treatment of FGFR4-driven cancer types. Western blot analysis revealed that (*R*)-**21c** suppressed FGF/FGFR and downstream signaling pathways at nanomolar concentrations. Furthermore, (*R*)-**21c** displayed potent antiproliferative effect against a number of FGFR-amplified cell lines including NCI-

H1581, KG1, SNU16, and RT112. After an oral administration of compound (*R*)-**21c** at a dose of 10 mg/kg/qd, almost complete tumor stasis was observed in nude mice bearing NCI-H1581 human lung cancer xenograft after 21 days of initial administration, indicating that (*R*)-**21c** was a potential FGFR inhibitor for further drug development.

Scheme 6[a]

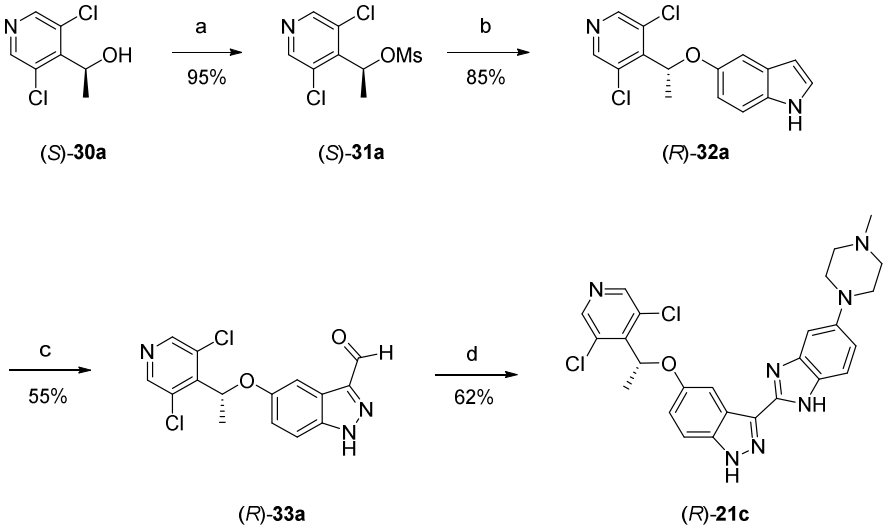

[a]Reagents and conditions: (a) MsCl, Et_3N, CH_2Cl_2, 0 °C to rt; (b) 5-hydroxyindole, Cs_2CO_3, DMF, 70 °C; (c) $NaNO_2$, HCl, H_2O/dioxane, 0 °C to rt; (d) (i) **40c**, H_2, 10% Pd/C, MeOH, rt; (ii) S_8, DMF, 90 °C.

EXPERIMENTAL SECTION

Chemistry.

All starting materials and reagents were either obtained from commercial suppliers or prepared according to literature reported procedures. All purchased chemicals and solvents were used without further purification unless otherwise noted. Flash chromatography was performed using silica gel (300−400 mesh). All reactions were monitored by thin-layer chromatography (TLC), using silica gel plates with fluorescence F254 and visualized under UV light. ^{1}H NMR spectral data were recorded on Varian Mercury 300 or 400 NMR spectrometer, and ^{13}C NMR was recorded on Varian Mercury 126 or

151 NMR spectrometer at ambient temperature. Chemicals shifts (δ) were reported in parts per million, coupling constants (J) values were in hertz, and the splitting patterns were abbreviated as follows: s for singlet; d for doublet; t for triplet; q for quartet and m for multiplet. The low or high resolution of EI-MS was recorded on a Finnigan/MAT95 spectrometer. All tested compounds were purified to ≥95% purity as determined by high performance liquid chromatography (HPLC).

General procedure A: Synthesis of target compounds 14–15, **16a and 16c.** A mixture of the aldehyde (**25a**–**e** or **33a**–**c**) (0.3 mmol), aniline (**28**, **34a** or **34c**) (0.3 mmol), and sulfur (0.6 mmol) was heated to 90 °C for 2 h under argon atmosphere[40]. Ethyl acetate was added and the reaction mixture was partitioned between ethyl acetate and water. The organic layer was washed with water and brine successively, dried over anhydrous sodium sulfate, and concentrated in vacuum. The resulting residue was purified by silica gel chromatography (dichloromethane/methanol + 2% of aqueous ammonia, v/v, 99:1 to 97:3) to give the desired product.

3-(5-(Piperidin-1-yl)-1*H*-benzo[*d*]imidazol-2-yl)-5-(pyridin-4-ylmethoxy)-1*H*-indazole (14a). The title compound was prepared from **25a** and **28** following general procedure A. Yellow solid (56%), mp 232 °C dec. ^{1}H NMR (300 MHz, CD_3OD) δ 8.54 (dd, J = 4.6, 1.6 Hz, 2H), 8.00 (d, J = 2.0 Hz, 1H), 7.57 (dd, J = 19.5, 7.6 Hz, 4H), 7.25 (dd, J = 9.1, 2.4 Hz, 2H), 7.08 (dd, J = 8.8, 2.1 Hz, 1H), 5.31 (s, 2H), 3.19–3.08 (m, 4H), 1.87–1.71 (m, 4H), 1.66–1.55 (m, 2H). ^{13}C NMR (126 MHz, acetone-d_6) δ 155.1, 152.1, 150.8 (2C), 150.5, 147.3, 139.9, 138.7, 137.5, 136.0, 122.7 (2C), 122.7, 120.1, 115.5, 112.3, 104.3, 103.1, 69.4, 53.2 (2C), 27.0 (2C), 25.1. HRMS (EI$^+$) m/z calcd for $C_{25}H_{24}N_6O$ 424.2012; found 424.2011.

5-((3-Chloropyridin-4-yl)methoxy)-3-(5-(piperidin-1-yl)-1*H*-benzo[*d*]imidazol-2-yl)-1*H*-indazole (14b). The title compound was prepared from **25b** and **28** following general procedure A. Yellow solid

(50%), mp 140–142 °C. ^{1}H NMR (300 MHz, CD_3OD) δ 8.59 (s, 1H), 8.51 (d, J = 5.0 Hz, 1H), 8.03 (s, 1H), 7.76 (d, J = 4.9 Hz, 1H), 7.58 (d, J = 3.6 Hz, 1H), 7.55 (d, J = 3.9 Hz, 1H), 7.30–7.23 (m, 2H), 7.10 (d, J = 8.8 Hz, 1H), 5.37 (s, 2H), 3.22–3.13 (m, 4H), 1.85–1.75 (m, 4H), 1.67–1.58 (m, 2H). ^{13}C NMR (151 MHz, acetone-d_6) δ 154.8, 149.8, 149.2, 147.6, 144.8, 139.9, 138.8, 138.6, 137.4, 130.8, 123.9, 122.6, 120.0 (2C), 116.2, 112.4, 104.5, 100.0, 67.1, 53.4 (2C), 26.8 (2C), 24.9. HRMS (EI^+) m/z calcd for $C_{25}H_{23}ClN_6O$ 458.1622; found 458.1619.

5-((3,5-Dichloropyridin-4-yl)methoxy)-3-(5-(piperidin-1-yl)-1*H*-benzo[*d*]imidazol-2-yl)-1*H*-indazole (14c). The title compound was prepared from **25c** and **28** following general procedure A. Yellow solid (72%), mp 205 °C dec. ^{1}H NMR (300 MHz, CD_3OD) δ 8.61 (s, 2H), 8.11 (d, J = 2.2 Hz, 1H), 7.64–7.50 (m, 2H), 7.30 (s, 1H), 7.19–7.09 (m, 2H), 5.45 (s, 2H), 3.26–3.14 (m, 4H), 1.89–1.75 (m, 4H), 1.68–1.57 (m, 2H). ^{13}C NMR (126 MHz, acetone-d_6) δ 155.3, 149.9 (2C), 148.9, 147.7, 141.2, 138.9, 137.3, 134.3 (2C), 122.6, 120.2, 116.3, 112.5, 104.3, 98.9, 65.5, 53.5 (2C), 26.7 (2C), 24.8. HRMS (EI^+) m/z calcd for $C_{25}H_{22}Cl_2N_6O$ 492.1232; found 492.1232.

3-(5-(Piperidin-1-yl)-1*H*-benzo[*d*]imidazol-2-yl)-5-(pyridin-3-ylmethoxy)-1*H*-indazole (14d). The title compound was prepared from **25d** and **28** following general procedure A. Yellow solid (54%), mp 152–154 °C. ^{1}H NMR (300 MHz, CD_3OD) δ 8.72 (s, 1H), 8.51 (d, J = 5.0 Hz, 1H), 8.08–7.97 (m, 2H), 7.63–7.45 (m, 3H), 7.28 (s, 1H), 7.22 (dd, J = 9.1, 2.2 Hz, 1H), 7.12 (dd, J = 8.8, 2.1 Hz, 1H), 5.30 (s, 2H), 3.24–3.15 (m, 4H), 1.86–1.74 (m, 4H), 1.69–1.57 (m, 2H). ^{13}C NMR (126 MHz, acetone-d_6) δ 155.3, 150.5, 150.3, 150.2, 147.7, 138.6, 137.5, 136.4, 133.9, 124.3, 122.7, 120.3, 116.2, 112.3, 104.1, 102.5, 68.8, 53.2 (2C), 27.0 (2C), 25.1. HRMS (EI^+) m/z calcd for $C_{25}H_{24}N_6O$ 424.2012; found 424.2004.

3-(5-(Piperidin-1-yl)-1*H*-benzo[*d*]imidazol-2-yl)-5-(pyridin-2-ylmethoxy)-1*H*-indazole (14e). The title compound was prepared from **25e** and **28** following general procedure A. Yellow solid (61%), mp 159–160 °C. ^{1}H NMR (300 MHz, CD_3OD) δ 8.57 (d, J = 4.9 Hz, 1H), 8.02 (d, J = 2.0 Hz, 1H), 7.90 (td, J = 7.7, 1.7 Hz, 1H), 7.70 (d, J = 7.9 Hz, 1H), 7.62–7.50 (m, 2H), 7.44–7.35 (m, 1H), 7.29–7.21 (m, 2H), 7.11 (dd, J = 8.8, 2.2 Hz, 1H), 5.32 (s, 2H), 3.25–3.11 (m, 4H), 1.89–1.74 (m, 4H), 1.69–1.56 (m, 2H). ^{13}C NMR (126 MHz, acetone-d_6) δ 158.4, 155.3, 150.1, 147.8, 138.6, 137.5, 137.3, 123.6, 122.8, 122.2, 120.1, 116.2, 112.3, 104.3, 101.7, 72.1, 53.5 (2C), 26.8 (2C), 24.9. HRMS (EI$^+$) m/z calcd for $C_{25}H_{24}N_6O$ 424.2012; found 424.2020.

5-(1-(3,5-Dichloropyridin-4-yl)ethoxy)-3-(5-(piperidin-1-yl)-1*H*-benzo[*d*]imidazol-2-yl)-1*H*-indazole (15a). The title compound was prepared from **33a** and **28** following general procedure A. Yellow solid (70%), mp 202 °C dec. ^{1}H NMR (300 MHz, acetone-d_6) δ 12.40 (s, 1H), 11.48 (s, 1H), 8.51 (s, 2H), 8.03 (s, 1H), 7.64 (s, 1H), 7.52 (d, J = 9.0 Hz, 1H), 7.18 (dd, J = 9.2, 1.9 Hz, 1H), 7.11–6.97 (m, 2H), 6.19 (q, J = 6.7 Hz, 1H), 3.22–3.08 (m, 4H), 1.85 (d, J = 6.6 Hz, 3H), 1.81–1.69 (m, 4H), 1.65–1.55 (m, 2H). ^{13}C NMR (126 MHz, acetone-d_6) δ 153.3, 149.7 (2C), 145.2, 141.3, 138.5, 137.5, 136.4, 132.0 (2C), 122.7, 120.3, 120.2, 115.5, 112.2, 105.1, 99.0, 72.9, 53.1 (2C), 27.0 (2C), 25.1, 19.0. HRMS (EI$^+$) m/z calcd for $C_{26}H_{24}Cl_2N_6O$ 506.1389; found 506.1390.

5-(1-(3,5-Dichloropyridin-4-yl)propoxy)-3-(5-(piperidin-1-yl)-1*H*-benzo[*d*]imidazol-2-yl)-1*H*-indazole (15b). The title compound was prepared from **33b** and **28** following general procedure A. Yellow solid (57%), mp 170 °C dec. ^{1}H NMR (400 MHz, CD_3OD) δ 8.41 (s, 2H), 7.84 (d, J = 2.1 Hz, 1H), 7.57 (d, J = 8.8 Hz, 1H), 7.46 (d, J = 9.0 Hz, 1H), 7.25 (s, 1H), 7.16 (dd, J = 9.0, 1.7 Hz, 1H), 7.09 (dd, J = 8.8, 2.0 Hz, 1H), 6.04–5.90 (m, 1H), 3.23–3.05 (m, 4H), 2.46–2.27 (m, 1H), 2.16–2.01 (m, 1H),

1.89–1.70 (m, 4H), 1.60 (d, J = 5.0 Hz, 2H), 1.13 (t, J = 7.4 Hz, 3H). HRMS (EI^+) m/z calcd for $C_{27}H_{26}Cl_2N_6O$ 520.1545; found 520.1544.

5-(1-(2,4-Dichloropyridin-3-yl)ethoxy)-3-(5-(piperidin-1-yl)-1*H*-benzo[*d*]imidazol-2-yl)-1*H*-indazole (15c). The title compound was prepared from **33c** and **28** following general procedure A. Beige solid (40%), mp 174 °C dec. ^{1}H NMR (300 MHz, CD_3OD) δ 8.12 (d, J = 5.3 Hz, 1H), 7.85 (d, J = 2.0 Hz, 1H), 7.57 (d, J = 8.4 Hz, 1H), 7.47 (d, J = 9.0 Hz, 1H), 7.39 (d, J = 5.1 Hz, 1H), 7.23 (s, 1H), 7.17 (dd, J = 9.0, 2.3 Hz, 1H), 7.09 (d, J = 8.6 Hz, 1H), 6.26 (q, J = 6.6 Hz, 1H), 3.21–3.12 (m, 3H), 1.89–1.75 (m, 6H), 1.69–1.57 (m, 2H). ^{13}C NMR (126 MHz, acetone-d_6) δ 153.4, 149.6 (2C), 145.3, 145.1, 138.9, 137.5, 137.2, 136.3, 132.1 (2C), 124.6, 123.0, 122.7, 120.2, 112.1, 107.9, 107.64, 103.9, 73.9, 51.8 (2C), 26.9 (2C), 25.6, 18.6. HRMS (EI^+) m/z calcd for $C_{26}H_{24}Cl_2N_6O$ 506.1389; found 506.1385.

3-(1*H*-Benzo[*d*]imidazol-2-yl)-5-(1-(3,5-dichloropyridin-4-yl)ethoxy)-1*H*-indazole (16a). The title compound was prepared from **33a** and *o*-phenylenediamine (**34a**) following general procedure A. White solid (79%), mp 222 °C dec. ^{1}H NMR (300 MHz, DMSO-d_6) δ 13.48 (s, 1H), 12.86 (s, 1H), 8.61 (s, 2H), 7.83 (d, J = 2.3 Hz, 1H), 7.78–7.72 (m, 1H), 7.55 (d, J = 9.0 Hz, 1H), 7.51–7.45 (m, 1H), 7.26–7.19 (m, 2H), 7.16 (dd, J = 9.0, 2.4 Hz, 1H), 6.10 (q, J = 6.6 Hz, 1H), 1.78 (d, J = 6.6 Hz, 3H). ^{13}C NMR (126 MHz, acetone-d_6) δ 153.5, 149.7 (2C), 148.2, 145.6, 145.2, 138.5, 137.1, 135.1, 132.0 (2C), 123.5, 122.8, 122.4, 120.4, 120.2, 112.4, 111.9, 104.8, 72.9, 19.1. HRMS (EI^+) m/z calcd for $C_{21}H_{15}Cl_2N_5O$ 423.0654; found 423.0653.

Synthesis of 2-(5-(1-(3,5-dichloropyridin-4-yl)ethoxy)-1*H*-indazol-3-yl)benzo[*d*]oxazole (16b). Compound **33a** (100 mg, 0.3 mmol) and 2-aminophenol (**34b**) (36 mg, 0.3 mmol) were dissolved in *N*,*N*-dimethylformamide (3 mL) and heated to 100 °C for 2 h. The mixture was concentrated to dryness

and dissolved in chloroform (2 mL). 2,3-Dichloro-5,6-dicyano-1,4-benzoquinone (150 mg, 0.66 mmol) was added and the solution was heated to reflux for 2 h.[41] The reaction mixture was diluted by chloroform and washed with water and brine successively, dried over anhydrous sodium sulfate, and concentrated in vacuum. The resulting residue was purified by silica gel chromatography (dichloromethane/methanol, v/v, 98:2) to give the title product as a yellow solid (80 mg, 63%), mp 232 °C dec. ^{1}H NMR (300 MHz, $CDCl_3$) δ 12.39 (s, 1H), 8.44 (s, 2H), 7.87–7.80 (m, 1H), 7.71 (d, J = 2.0 Hz, 1H), 7.65–7.60 (m, 1H), 7.57 (d, J = 9.1 Hz, 1H), 7.46–7.36 (m, 2H), 7.20 (dd, J = 9.1, 2.4 Hz, 1H), 6.17 (q, J = 6.7Hz, 1H), 1.85 (d, J = 6.7 Hz, 3H). ^{13}C NMR (126 MHz, acetone-d_6) δ 159.5, 154.2, 151.0, 149.8 (2C), 145.0, 143.0, 138.3, 133.7, 132.0 (2C), 126.1, 125.6, 123.5, 120.8, 113.0, 111.5, 103.6, 73.0, 19.0. HRMS (EI$^+$) m/z calcd for $C_{21}H_{14}Cl_2N_4O_2$ 424.0494; found 424.0503.

2-(5-(1-(3,5-Dichloropyridin-4-yl)ethoxy)-1*H*-indazol-3-yl)benzo[*d*]thiazole (16c). The title compound was prepared from **33a** and 2-aminobenzenethiol (**34c**) following general procedure A. Beige solid (35%), mp 220 °C dec. ^{1}H NMR (300 MHz, acetone-d_6) δ 12.69 (s, 1H), 8.55 (s, 2H), 8.21 (d, J = 8.6 Hz, 1H), 8.07 (d, J = 8.0 Hz, 1H), 7.85 (d, J = 2.3 Hz, 1H), 7.65–7.55 (m, 2H), 7.46 (t, J = 7.6 Hz, 1H), 7.24 (dd, J = 9.0, 2.5 Hz, 1H), 6.20 (q, J = 6.7 Hz, 1H), 1.86 (d, J = 6.7 Hz, 3H). ^{13}C NMR (126 MHz, acetone-d_6) δ 162.9, 155.2, 154.2, 149.7 (2C), 145.1, 140.0, 138.8, 134.9, 131.9 (2C), 127.1, 126.2, 123.8, 122.7, 122.0, 121.0, 112.9, 103.6, 72.8, 19.1. HRMS (EI$^+$) m/z calcd for $C_{21}H_{14}Cl_2N_4OS$ 440.0265; found 440.0262.

Synthesis of 5-(1-(3,5-dichloropyridin-4-yl)ethoxy)-3-(1*H*-indol-2-yl)-1*H*-indazole (17). Compounds **35** (72 mg, 0.14 mmol) and **36** (40 mg, 0.15 mmol) were dissolved in dioxane (5 mL) and cesium carbonate (91 mg, 0.28 mmol) was added. The suspension was degassed under argon bubbling for 10 min before $Pd(dppf)_2Cl_2$ (7 mg, 0.01 mmol) was added. The reaction mixture was heated to 90 °C

for 2 h and then diluted with ethyl acetate. The solution was washed with water and brine successively, dried over anhydrous sodium sulfate, and concentrated in vacuum. The resulting residue was dissolved in a solution of hydrochloric acid in methanol (0.5 mL, 4 N) and the mixture was continually stirred overnight at room temperature. The mixture was concentrated and purified by silica gel chromatography (dichloromethane/methanol, v/v, 98:2) to give the title product as a light brown solid (34 mg, 58%), mp 216 °C dec. ^{1}H NMR (400 MHz, $CDCl_3$) δ 9.96 (s, 1H), 9.05 (s, 1H), 8.45 (s, 2H), 7.71 (d, J = 7.5 Hz, 1H), 7.43–7.36 (m, 2H), 7.30 (s, 1H), 7.25–7.21 (m, 1H), 7.20–7.13 (m, 2H), 6.97 (s, 1H), 6.14 (q, J = 6.8 Hz, 1H), 1.86 (d, J = 6.7 Hz, 3H). ^{13}C NMR (126 MHz, $CDCl_3$) δ 152.5, 149.1 (2C), 144.4, 138.8, 137.7, 136.0, 131.3 (2C), 131.0, 129.2, 122.9, 120.8, 120.2, 119.9, 111.3, 111.0, 102.8, 100.9, 72.2, 18.9. HRMS (EI^+) m/z calcd for $C_{22}H_{16}Cl_2N_4O$ 422.0701; found 422.0701.

General procedure B: Synthesis of target compounds 18–22. The substituted 2-nitroaniline (**26**, **37**– **38** or **40**–**41**) (0.3 mmol) was dissolved in methanol (3 mL) and 10% Pd/C (0.03 mmol) was added. The mixture was stirred at room temperature under hydrogen atmosphere for 2 h. The mixture was filtered and the filtrate was concentrated to dryness and dissolved in *N*,*N*-dimethylformamide (3 mL). Compound **33a** (0.3 mmol) and sulfur (0.6 mmol) was added. The mixture was heated to 90 °C for 2 h under argon atmosphere. Ethyl acetate was added and the reaction mixture was partitioned between ethyl acetate and water. The organic layer was washed with water and brine successively, dried over anhydrous sodium sulfate, and concentrated in vacuum. The resulting residue was purified by silica gel chromatography (dichloromethane/methanol + 2% of aqueous ammonia, v/v, 99:1 to 95:5) to give the desired product.

5-(1-(3,5-Dichloropyridin-4-yl)ethoxy)-3-(4-methyl-1*H*-benzo[*d*]imidazol-2-yl)-1*H*-indazole (18a). The title compound was prepared from **37a** following general procedure B. Beige solid (51%),

mp 137–139 °C. ^{1}H NMR (300 MHz, CD_3OD) δ 8.42 (s, 2H), 7.73 (s, 1H), 7.49 (d, J = 9.0 Hz, 1H), 7.36 (s, 1H), 7.23–7.12 (m, 2H), 7.05 (d, J = 7.2 Hz, 1H), 6.21 (q, J = 6.7 Hz, 1H), 2.74–2.62 (m, 3H), 1.82 (d, J = 6.7 Hz, 3H).

5-(1-(3,5-Dichloropyridin-4-yl)ethoxy)-3-(4-(piperidin-1-yl)-1*H*-benzo[*d*]imidazol-2-yl)-1*H*-indazole (18b). The title compound was prepared from **37b** following general procedure B. Brown solid (43%), mp 120–122 °C. ^{1}H NMR (300 MHz, DMSO-d_6) δ 13.45 (s, 1H), 12.76 (s, 1H), 8.56 (s, 2H), 8.08 (s, 1H), 7.54 (d, J = 9.1 Hz, 1H), 7.20 (d, J = 8.7 Hz, 1H), 7.05 (t, J = 7.7 Hz, 1H), 6.98 (d, J = 7.7 Hz, 1H), 6.53 (d, J = 7.5 Hz, 1H), 6.20 (dd, J = 12.6, 6.4 Hz, 1H), 3.72–3.50 (m, 4H), 1.90–1.72 (m, 7H), 1.68–1.66 (m, 2H). ^{13}C NMR (126 MHz, CD_3OD) δ 154.0, 149.7 (2C), 147.0, 146.2, 139.2, 138.3, 137.0, 132.8 (2C), 130.3, 124.5, 122.9, 120.9, 112.4, 110.7, 106.7, 74.2, 53.6 (2C), 27.1 (2C), 25.5, 18.7. HRMS (EI$^+$) m/z calcd for $C_{26}H_{24}Cl_2N_6O$ 506.1389; found 506.1387.

5-(1-(3,5-Dichloropyridin-4-yl)ethoxy)-3-(5-fluoro-1*H*-benzo[*d*]imidazol-2-yl)-1*H*-indazole (19a). The title compound was prepared from **26a** following general procedure B. White solid (72%), mp >250 °C. ^{1}H NMR (300 MHz, DMSO-d_6) δ 13.53–13.51 (m, 1H), 12.99 (s, 1H), 8.62–8.61 (m, 2H), 7.78 (s, 1H), 7.74–7.43 (m, 1H), 7.55 (d, J = 8.1 Hz, 1H), 7.51–7.19 (m, 1H), 7.16 (dd, J = 9.0, 2.4 Hz, 1H), 7.11–7.04 (m,1H), 6.10 (q, J = 6.7 Hz, 1H), 1.78 (d, J = 6.7 Hz, 3H). HRMS (EI$^+$) m/z calcd for $C_{21}H_{14}Cl_2FN_5O$ 441.0559; found 441.0562.

5-(1-(3,5-Dichloropyridin-4-yl)ethoxy)-3-(5-methyl-1*H*-benzo[*d*]imidazol-2-yl)-1*H*-indazole (19b). The title compound was prepared from **26b** following general procedure B. White solid (55%), mp 215 °C dec. ^{1}H NMR (300 MHz, CD_3OD) δ 8.43 (s, 2H), 7.81 (s, 1H), 7.67–7.32 (m, 3H), 7.17 (dd, J = 9.0, 2.1 Hz, 1H), 7.11 (d, J = 7.8 Hz, 1H), 6.24 (q, J = 6.6 Hz, 1H), 2.50 (s, 3H), 1.83 (d, J = 6.6 Hz, 3H). ^{13}C NMR (126 MHz, CD_3OD) δ 154.1, 149.8 (2C), 148.5, 146.3, 139.1, 136.9, 133.7, 132.7 (2C),

125.2, 122.7, 120.9, 116.0, 112.5, 104.87, 73.65, 21.78, 18.92. HRMS (EI^+) *m*/*z* calcd for $C_{22}H_{17}Cl_2N_5O$ 437.0810; found 437.0810.

5-(1-(3,5-Dichloropyridin-4-yl)ethoxy)-3-(5-methoxy-1*H*-benzo[*d*]imidazol-2-yl)-1*H*-indazole (19c). The title compound was prepared from **26c** following general procedure B. Yellow solid (58%), mp 150 °C dec. ^{1}H NMR (300 MHz, CD_3OD) δ 8.43 (s, 2H), 7.81 (d, J = 1.9 Hz, 1H), 7.55 (d, J = 8.8 Hz, 1H), 7.47 (d, J = 9.0 Hz, 1H), 7.21–7.12 (m, 2H), 6.92 (dd, J = 8.8, 2.3 Hz, 1H), 6.23 (q, J = 6.5 Hz, 1H), 3.88 (s, 3H), 1.83 (d, J = 6.6 Hz, 3H). HRMS (EI^+) *m*/*z* calcd for $C_{22}H_{17}Cl_2N_5O_2$ 453.0759; found 453.0751.

2-(5-(1-(3,5-Dichloropyridin-4-yl)ethoxy)-1*H*-indazol-3-yl)-*N*-methyl-1*H*-benzo[*d*]imidazol-5-amine (19d). The title compound was prepared from **26d** following general procedure B. Yellow solid (62%), mp 182 °C dec. ^{1}H NMR (300 MHz, DMSO-d_6) δ 13.29 (s, 1H), 12.29 (s, 1H), 8.60 (s, 2H), 7.81 (s, 1H), 7.50 (d, J = 9.0 Hz, 1H), 7.41 (s, 1H), 7.12 (dd, J = 9.0, 2.4 Hz, 1H), 6.58 (dd, J = 8.7, 2.0 Hz, 1H), 6.49 (s, 1H), 6.08 (q, J = 6.7 Hz, 1H), 5.61 (s, 1H), 2.73 (s, 3H), 1.78 (d, J = 6.7 Hz, 3H). ^{13}C NMR (126 MHz, acetone-d_6) δ 153.3, 149.6 (2C), 147.8, 145.9, 145.3, 138.5, 137.4, 132.0 (2C), 122.5, 120.2, 118.5, 112.1, 112.0, 105.2, 94.7, 73.0, 31.4, 19.0. HRMS (EI^+) *m*/*z* calcd for $C_{22}H_{18}Cl_2N_6O$ 452.0919; found 452.0907.

***N*-(2-(5-(1-(3,5-Dichloropyridin-4-yl)ethoxy)-1*H*-indazol-3-yl)-1*H*-benzo[*d*]imidazol-6-yl)-2-(dimethylamino)-*N*-methylacetamide (19e).** To a mixture of **19d** (50 mg, 0.11 mmol) and triethylamine (30 μL, 0.22 mmol) in *N*,*N*-dimethylformamide (2 mL), 2-bromoacetyl chloride (10 μL, 0.13 mmol) was added dropwise at 0 °C. The reaction mixture was stirred at room temperature for 3 h and concentrated before a solution of dimethylamine in THF (5 mL, 2 N) was added. The mixture was stirred overnight at room temperature and was concentrated. The resulting residue was purified by silica

gel chromatography (dichloromethane/methanol + 2% of aqueous ammonia, v/v, 96:4) to give the title compound as a beige solid (26 mg, 45%), mp 185 °C dec. ^{1}H NMR (300 MHz, CD_3OD) δ 8.45 (s, 2H), 7.83 (s, 1H), 7.73 (s, 1H), 7.56 (s, 1H), 7.50 (d, J = 9.1 Hz, 1H), 7.24–7.13 (m, 2H), 6.23 (q, J = 6.7 Hz, 1H), 3.35 (s, 3H), 3.03 (s, 2H), 2.25 (s, 6H), 1.84 (d, J = 6.7 Hz, 3H). HRMS (EI^+) m/z calcd for $C_{26}H_{25}Cl_2N_7O_2$ 537.1447; found 537.1454.

5-(1-(3,5-Dichloropyridin-4-yl)ethoxy)-3-(5-(1-methylpiperidin-4-yl)-1*H*-benzo[*d*]imidazol-2-yl)-1*H*-indazole (20). The title compound was prepared from **38** following general procedure B. Beige solid (49%), mp 162–163 °C. ^{1}H NMR (300 MHz, CD_3OD) δ 8.43 (s, 2H), 7.83 (d, J = 1.4 Hz, 1H), 7.58 (s, 1H), 7.56–7.44 (m, 2H), 7.23–7.13 (m, 2H), 6.23 (q, J = 6.6 Hz, 1H), 3.04 (d, J = 10.9 Hz, 2H), 2.76–2.63 (m, 1H), 2.35 (s, 3H), 2.29–2.14 (m, 2H), 2.00–1.78 (m, 7H). ^{13}C NMR (126 MHz, CD_3OD) δ 154.1, 149.8 (2C), 148.9, 146.3, 142.4, 139.1, 136.8, 132.7 (2C), 123.2, 122.8, 120.9, 116.1, 112.5, 104.9, 73.7, 57.3 (2C), 46.4, 43.2, 34.7 (2C), 18.9. HRMS (EI^+) m/z calcd for $C_{27}H_{26}Cl_2N_6O$ 520.1545; found 520.1550.

3-(5-([1,4'-Bipiperidin]-1'-yl)-1*H*-benzo[*d*]imidazol-2-yl)-5-(1-(3,5-dichloropyridin-4-yl)ethoxy)-1*H*-indazole (21a). The title compound was prepared from **40a** following general procedure B. Yellow solid (45%), mp 185 °C dec. ^{1}H NMR (300 MHz, CD_3OD) δ 8.43 (s, 2H), 7.83 (s, 1H), 7.56 (d, J = 9.4 Hz, 1H), 7.47 (d, J = 9.2 Hz, 1H), 7.18–7.14 (m, 2H), 7.07 (d, J = 9.0 Hz, 1H), 6.24 (q, J = 6.7 Hz, 1H), 3.72 (d, J = 11.4 Hz, 2H), 2.72 (t, J = 12.0 Hz, 2H), 2.66–2.55 (m, 4H), 2.41 (t, J = 10.2 Hz, 1H), 2.00 (d, J = 9.9 Hz, 2H), 1.84 (d, J = 6.7 Hz, 3H), 1.75 (d, J = 11.1 Hz, 2H), 1.70–1.57 (m, 4H), 1.51–1.47 (m, 2H). HRMS (EI^+) m/z calcd for $C_{31}H_{33}Cl_2N_7O$ 589.2124; found 589.2121.

5-(1-(3,5-Dichloropyridin-4-yl)ethoxy)-3-(5-((3*S*,5*R*)-3,5-dimethylpiperazin-1-yl)-1*H*-benzo[*d*]imidazol-2-yl)-1*H*-indazole (21b). The title compound was prepared from **40b** following

general procedure B. Yellow solid (44%), mp 182–183 °C. ^{1}H NMR (300 MHz, CD_3OD) δ 8.43 (s, 2H), 7.82 (s, 1H), 7.59 (s, 1H), 7.47 (d, J = 9.2 Hz, 1H), 7.26–7.14 (m, 2H), 7.09 (d, J = 8.9 Hz, 1H), 6.23 (q, J = 6.5 Hz, 1H), 3.62 (d, J = 11.3 Hz, 2H), 3.28–3.13 (m, 2H), 2.45 (t, J = 11.4 Hz, 2H), 1.83 (d, J = 6.6 Hz, 3H), 1.25 (d, J = 6.4 Hz, 6H). HRMS (EI$^+$) m/z calcd for $C_{27}H_{27}Cl_2N_7O$ 535.1654; found 535.1647.

5-(1-(3,5-Dichloropyridin-4-yl)ethoxy)-3-(5-(4-methylpiperazin-1-yl)-1*H*-benzo[*d*]imidazol-2-yl)-1*H*-indazole (21c). The title compound was prepared from **40c** following general procedure B. Beige solid (68%), mp 190 °C dec. ^{1}H NMR (300 MHz, CD_3OD) δ 8.41 (s, 2H), 7.82 (s, 1H), 7.57 (d, J = 8.7 Hz, 1H), 7.46 (d, J = 9.0 Hz, 1H), 7.21–7.13 (m, 2H), 7.05 (d, J = 8.8 Hz, 1H), 6.21 (q, J = 6.7 Hz, 1H), 3.29–3.21 (m, 4H), 2.82–2.71 (m, 4H), 2.44 (s, 3H), 1.81 (d, J = 6.6 Hz, 3H). ^{13}C NMR (101 MHz, acetone-d_6) δ 153.3, 149.7 (2C), 145.2, 140.3, 138.5, 137.4, 135.1, 132.0 (2C), 122.7, 120.3, 120.5, 114.8, 112.3, 105.1, 98.9, 72.9, 55.8 (2C), 51.1 (2C), 45.9, 19.0. HRMS (EI$^+$) m/z calcd for $C_{26}H_{25}Cl_2N_7O$ 521.1498; found 521.1493.

5-(1-(3,5-Dichloropyridin-4-yl)ethoxy)-3-(5-(4-ethylpiperazin-1-yl)-1*H*-benzo[*d*]imidazol-2-yl)-1*H*-indazole (21d). The title compound was prepared from **40d** following general procedure B. Yellow solid (58%), mp 185–186 °C. ^{1}H NMR (300 MHz, CD_3OD) δ 8.43 (s, 2H), 7.82 (s, 1H), 7.62 (s, 1H), 7.48 (d, J = 8.9 Hz, 1H), 7.22–7.04 (m, 3H), 6.24 (q, J = 6.7 Hz, 1H), 3.30–3.23 (m, 4H), 2.78–2.67 (m, 4H), 2.55 (q, J = 7.3 Hz, 2H), 1.84 (d, J = 6.6 Hz, 3H), 1.18 (t, J = 7.2 Hz, 3H). HRMS (EI$^+$) m/z calcd for $C_{27}H_{27}Cl_2N_7O$ 535.1654; found 535.1651.

4-(2-(5-(1-(3,5-Dichloropyridin-4-yl)ethoxy)-1*H*-indazol-3-yl)-1*H*-benzo[*d*]imidazol-5-yl)morpholine (21e). The title compound was prepared from **40e** following general procedure B. Beige solid (52%), mp 185 °C dec. ^{1}H NMR (300 MHz, acetone-d_6) δ 12.51 (s, 1H), 8.51 (s, 2H), 8.04 (d, J = 2.2 Hz, 1H), 7.62 (d, J = 8.6 Hz, 1H), 7.53 (d, J = 9.0 Hz, 1H), 7.24–7.14 (m, 2H), 7.05 (dd, J = 8.8, 1.8

Hz, 1H), 6.20 (q, *J* = 6.5 Hz, 1H), 3.88–3.79 (m, 4H), 3.21–3.13 (m, 4H), 1.84 (d, *J* = 6.6 Hz, 3H). HRMS (EI^+) *m*/*z* calcd for $C_{25}H_{22}Cl_2N_6O_2$ 508.1181; found 508.1179.

5-(1-(3,5-Dichloropyridin-4-yl)ethoxy)-3-(5-(4-methyl-1,4-diazepan-1-yl)-1*H*-benzo[*d*]imidazol-2-yl)-1*H*-indazole (21f). The title compound was prepared from **40f** following general procedure B. Yellow solid (57%), mp 145–147 °C. ^{1}H NMR (300 MHz, CD_3OD) δ 8.41 (s, 2H), 7.82 (s, 1H), 7.60–7.42 (m, 2H), 7.15 (d, *J* = 9.0 Hz, 1H), 6.93–6.78 (m, 2H), 6.21 (q, *J* = 6.7 Hz, 1H), 3.70–3.61 (m, 2H), 3.54 (t, *J* = 6.2 Hz, 2H), 2.93–2.85 (m, 2H), 2.77–2.69 (m, 2H), 2.45 (s, 3H), 2.16–2.04 (m, 2H), 1.81 (d, *J* = 6.6 Hz, 3H). HRMS (EI^+) *m*/*z* calcd for $C_{27}H_{27}Cl_2N_7O$ 535.1654; found 535.1650.

***N*^{1}-(2-(5-(1-(3,5-Dichloropyridin-4-yl)ethoxy)-1*H*-indazol-3-yl)-1*H*-benzo[*d*]imidazol-5-yl)-*N*^{2},*N*^{2}-dimethylethane-1,2-diamine (21g).** The title compound was prepared from **40g** following general procedure B. Yellow solid (48%), mp 140–142 °C. ^{1}H NMR (300 MHz, CD_3OD) δ 8.42 (s, 2H), 7.80 (s, 1H), 7.54–7.41 (m, 2H), 7.15 (d, *J* = 10.1 Hz, 1H), 6.81 (s, 1H), 6.73 (d, *J* = 8.7 Hz, 1H), 6.22 (q, *J* = 6.6 Hz, 1H), 3.30 (t, *J* =6.3 Hz, 2H), 2.64 (t, *J* = 6.3 Hz, 2H), 2.33 (s, 6H), 1.82 (d, *J* = 6.7 Hz, 3H). HRMS (EI^+) *m*/*z* calcd for $C_{25}H_{25}Cl_2N_7O$ 509.1498; found 509.1503.

2-(5-(1-(3,5-Dichloropyridin-4-yl)ethoxy)-1*H*-indazol-3-yl)-*N*-(2-methoxyethyl)-1*H*-benzo[*d*]imidazol-5-amine (21h). The title compound was prepared from **40h** following general procedure B. Yellow solid (55%), mp 132–133 °C. ^{1}H NMR (300 MHz, CD_3OD) δ 8.42 (s, 2H), 7.80 (d, *J* = 1.8 Hz, 1H), 7.51–7.40 (m, 2H), 7.15 (dd, *J* = 9.0, 2.1 Hz, 1H), 6.85 (s, 1H), 6.76 (dd, *J* = 8.7, 1.8 Hz, 1H), 6.22 (q, *J* = 6.7 Hz, 1H), 3.64 (t, *J* = 5.4 Hz, 2H), 3.40 (s, 3H), 3.34 (t, *J* = 5.4 Hz, 2H), 1.82 (d, *J* = 6.6 Hz, 3H). HRMS (EI^+) *m*/*z* calcd for $C_{24}H_{22}Cl_2N_6O_2$ 496.1181; found 496.1171.

2-(2-(5-(1-(3,5-Dichloropyridin-4-yl)ethoxy)-1*H*-indazol-3-yl)-1*H*-benzo[*d*]imidazol-5-yl)ethan-1-ol (22). The title compound was prepared from **41** following general procedure B. White solid (77%), mp 150–151 °C. ^{1}H NMR (300 MHz, CD_3OD) δ 8.42 (s, 2H), 7.82 (d, J = 2.2 Hz, 1H), 7.59 (s, 1H), 7.55–7.44 (m, 2H), 7.21–7.13 (m, 2H), 6.23 (q, J = 6.7 Hz, 1H), 3.84 (t, J = 7.1 Hz, 2H), 3.35 (s, 1H), 2.98 (t, J = 7.1 Hz, 2H), 1.82 (d, J = 6.7 Hz, 3H). ^{13}C NMR (126 MHz, CD_3OD) δ 154.1, 149.8 (2C), 148.8, 146.3, 139.1, 136.8, 135.0, 132.7 (2C), 125.0, 122.8, 120.9, 119.4, 112.5, 104.9, 73.7, 64.8, 40.6, 18.9. HRMS (EI^+) m/z calcd for $C_{23}H_{19}Cl_2N_5O_2$ 467.0916; found 467.0918.

General procedure C: Synthesis of ethers 24a–e and 32a–c. 5-Hydroxyindole (1.1 mmol) and cesium carbonate (1.2 mmol) in *N*,*N*-dimethylformamide (10 mL) was heated to 70 °C. Benzyl chloride (**23a–e**) or methanesulfonate (**31a–c**) (1 mmol) was added and the mixture was stirred for 2 h. Water was added and the reaction mixture was partitioned between ethyl acetate and water. The organic layer was washed with water and brine successively, dried over anhydrous sodium sulfate, and concentrated in vacuum. The resulting residue was purified by silica gel chromatography (petroleum ether/ethyl acetate, v/v, 90:10) to give the desired product.

General procedure D: Synthesis of aldehydes 25a–e and 33a–c. 5-Substituted indole (**24a–e, 32a–c**) (0.58 mmol) was dissolved in water (6 mL) and dioxane (6 mL). Sodium nitrite (5.8 mmol) was added and the solution was cooled to 0 °C. Hydrochloric acid (3 mL, 3 N) was added dropwise over 5 min and the resulting mixture was then stirred at room temperature for additional 3 h. Ethyl acetate was added and the reaction mixture was partitioned between ethyl acetate and water. The organic layer was washed with water and brine successively, dried over anhydrous sodium sulfate, and concentrated in vacuum. The resulting residue was purified by silica gel chromatography (petroleum ether/dichloromethane, v/v, 90:10) to give the desired product.[34]

General procedure E: Synthesis of substituted 2-nitroanilines 26d, 27 and 40a–h. A mixture of 5-fluoro-2-nitroaniline (**26a**) (468 mg, 3 mmol), *N*,*N*-diisopropylethylamine (1.4 mL, 7.5 mmol) and nucleophiles in *N*-methyl-2-pyrrolidone (20 mL) was heated to 120 °C for 4 h. The reaction mixture was poured into water and extracted with ethyl acetate. The organic layer was washed with water and brine successively, dried over anhydrous sodium sulfate, and concentrated in vacuum. The resulting residue was purified by silica gel chromatography (dichloromethane/methanol, v/v, 97:3) to give the desired product.

Chiral synthesis of (*R*)-21c

Step 1: (*S*)-1-(3,5-dichloropyridin-4-yl)ethan-1-ol ((*S*)-30a). A mixture of **30a** (3.6 g, 18.8 mmol), (*R*)-2-(2,4-dichlorophenoxy)propanoic acid[42] (**42**) (2.2 g, 9.4 mmol), and 4-dimethylaminopyridine (114 mg, 0.94 mmol) was dissolved in anhydrous toluene (100 mL). Dicyclohexylcarbodiimide (1.94 g, 9.4 mmol) was added slowly to the mixture at 0 °C. The resulting slurry was stirred at ambient temperature for 20 min and filtered. The filtrate was concentrated in vacuum and purified by silica gel chromatography (petroleum ether/ethyl acetate, v/v, 95:5) to give the corresponding ester as a pale yellow oil (3.8 g, 49%). The resulting ester was dissolved in ethanol (40 mL) and aqueous sodium hydroxide (24 mL, 2 N) was added. The reaction mixture was stirred at ambient temperature for 2 h, then the solvent was evaporated in vacuum. The mixture was partitioned between water and dichloromethane. The organic layer was washed with brine, dried over anhydrous sodium sulfate, and concentrated in vacuum to give (*S*)-**30a'** as a colorless oil (1.75 g, 98%). The aqueous layer was acidified to pH=2 with 2 N HCl and filtered, the filter cake was collected and dried to retrieve **42** as a white solid (2.1 g, 98%). The above mentioned method was repeated once to give (*S*)-**30a** as a colorless oil (830 mg, 23% for two steps). $[\alpha]^{20}_{D}$ = +12.07 (*c* 0.340, methanol) (98% ee, CHIRALPAK AD-H, *n*-

Heptane: EtOH=90: 10, flow rate 1.0 mL/min, t_R= 10.1 min, peak 2)[36]. ^{1}H NMR (300 MHz, $CDCl_3$) δ 8.44 (s, 2H), 5.59–5.46 (m, 1H), 2.82 (d, J = 9.6 Hz, 1H), 1.63 (d, J = 7.8 Hz, 3H).

Step 2: (*S*)-1-(3,5-dichloropyridin-4-yl)ethyl methanesulfonate ((*S*)-31a). Compound (*S*)-**30a** (800 mg, 4.2 mmol) and triethylamine (0.88 mL, 6.2 mmol) were dissolved in anhydrous dichloromethane (20 mL). Methanesulfonyl chloride (0.5 mL, 6.2 mmol) was added dropwise at 0 °C. After the addition was complete, the resulting mixture was stirred at room temperature for 2 h. Water was added and the reaction mixture was partitioned between dichloromethane and water. The organic layer was washed with water and brine successively, dried over anhydrous sodium sulfate, and concentrated in vacuum to give the title product as a white solid (1.1 g, 95%). Mp: 46–48 °C. $[\alpha]^{20}_D$ = −40.06 (*c* 0.304, methanol). ^{1}H NMR (300 MHz, $CDCl_3$) δ 8.51 (s, 2H), 6.36 (q, J = 6.9 Hz, 1H), 2.97 (s, 3H), 1.81 (d, J = 6.9 Hz, 3H).

Step 3: (*R*)-5-(1-(3,5-dichloropyridin-4-yl)ethoxy)-1*H*-indole ((*R*)-32a). The title compound was prepared from (*S*)-**31a** following general procedure C. Colorless oil (85%). $[\alpha]^{20}_D$ = +47.66 (*c* 0.107, methanol) (89% ee, CHIRALPAK AD-H, *n*-Hexane: *i*-prOH=90: 10, flow rate 1.0 mL/min, t_R= 18.8 min). ^{1}H NMR (400 MHz, $CDCl_3$) δ 8.40 (s, 2H), 8.11 (s, 1H), 7.23 (d, J = 8.8 Hz, 1H), 7.14 (t, J = 2.8 Hz, 1H), 6.99 (d, J = 2.4 Hz, 1H), 6.88 (dd, J = 8.8, 2.4 Hz, 1H), 6.41–6.39 (m, 1H), 6.02 (q, J = 6.7 Hz, 1H), 1.79 (d, J = 6.7 Hz, 3H).

Step 4: (*R*)-5-(1-(3,5-dichloropyridin-4-yl)ethoxy)-1*H*-indazole-3-carbaldehyde ((*R*)-33a). The title compound was prepared from (*R*)-**32a** following general procedure D. The obtained solid was suspended in ethyl acetate and stirred for 30 min. The slurry was filtered and the filter cake was dried in vacuum to give (*R*)-**33a**. Yellow solid (55%). Mp: 188 °C dec. $[\alpha]^{20}_D$ = +76.33 (*c* 0.207, methanol) (99% ee, CHIRALPAK AD-H, *n*-Hexane: *i*-prOH=90: 10, flow rate 1.0 mL/min, t_R= 18.2 min). ^{1}H NMR (300

MHz, $CDCl_3$) δ 10.13 (s, 1H), 8.37 (s, 2H), 7.52 (s, 1H), 7.41 (d, J = 9.0 Hz, 1H), 7.13 (d, J = 9.1 Hz, 1H), 6.07 (q, J = 6.7 Hz, 1H), 1.78 (d, J = 6.7 Hz, 3H).

Step 5: (*R*)-5-(1-(3,5-dichloropyridin-4-yl)ethoxy)-3-(5-(4-methylpiperazin-1-yl)-1*H*-benzo[*d*]imidazol-2-yl)-1*H*-indazole ((*R*)-21c). The title compound was prepared from (*R*)-**33a** following general procedure B. Pale yellow solid (62%). Mp: 199 °C dec. $[\alpha]^{20}_{D}$ = +229.29 (*c* 0.218, methanol) (99% ee, CHIRALPAK IE, *n*-Hexane: EtOH: diethylamine =70: 30: 0.1 (v/v/v), flow rate 0.8 mL/min, t_R= 20.7 min). ^{1}H NMR (300 MHz, CD_3OD) δ 8.41 (s, 2H), 7.82 (s, 1H), 7.57 (d, J = 8.7 Hz, 1H), 7.46 (d, J = 9.0 Hz, 1H), 7.21–7.13 (m, 2H), 7.05 (d, J = 8.8 Hz, 1H), 6.21 (q, J = 6.7 Hz, 1H), 3.29–3.21 (m, 4H), 2.82–2.71 (m, 4H), 2.44 (s, 3H), 1.81 (d, J = 6.6 Hz, 3H). ^{13}C NMR (101 MHz, acetone-d_6) δ 153.3, 149.7 (2C), 145.2, 140.3, 138.5, 137.4, 135.1, 132.0 (2C), 122.7, 120.3, 120.5, 114.8, 112.3, 105.1, 98.9, 72.9, 55.8 (2C), 51.1 (2C), 45.9, 19.0. HRMS (EI^+) m/z calcd for $C_{26}H_{25}Cl_2N_7O$ 521.1498; found 521.1493.

Kinase profiling

The kinase profiling of (*R*)-**21c** was conducted using Elisa kinase assay and the Eurofins Kinase Profiler Selectivity Testing Service.

Elisa kinase assay: The effects of indicated compounds on the activities of various tyrosine kinases were determined using enzyme-linked immunosorbent assays (ELISAs) with purified recombinant proteins. Briefly, 20 μg/mL poly (Glu, Tyr) 4:1 (Sigma, St Louis, MO, USA) was pre-coated in 96-well plates as a substrate. A 50-μL aliquot of 10 μM ATP solution diluted in kinase reaction buffer (50 mM HEPES [pH 7.4], 50 mM $MgCl_2$, 0.5 mM $MnCl_2$, 0.2 mM Na_3VO_4, and 1 mM DTT) was added to each well; 1 μL of various concentrations of indicated compounds diluted in 1% DMSO (v/v) (Sigma, St Louis, MO, USA) were then added to each reaction well. DMSO (1%, v/v) was used as the negative

control. The kinase reaction was initiated by the addition of purified tyrosine kinase proteins (FGFR1, FGFR2, FGFR3, FGFR4, VEGFR2, EGFR, ErbB2, PDGFRα, PDGFRβ, c-Met, Flt1, Flt3, RET , c-Src ,Bcr-Abl and EPHA2) diluted in 49 μL of kinase reaction buffer. After incubation for 60 min at 37 °C, the plate was washed for three times with phosphate-buffered saline (PBS) containing 0.1% Tween 20 (T-PBS). Anti-phosphotyrosine (PY99) antibody (100 μL; 1:500, diluted in 5 mg/mL BSA T-PBS) was then added. After a 30-min incubation at 37 °C, the plate was washed for three times, and 100 μL horseradish peroxidase-conjugated goat anti-mouse IgG (1:1000, diluted in 5 mg/mL BSA T-PBS) was added. The plate was then incubated at 37 °C for 30 min and washed for three times. A 100-μL aliquot of a solution containing 0.03% H_2O_2 and 2 mg/mL o-phenylenediamine in 0.1 M citrate buffer (pH 5.5) was added. The reaction was terminated by the addition of 50 μL of 2 M H_2SO_4 as the color changed, and the plate was analyzed using a multi-well spectrophotometer (SpectraMAX190, from Molecular Devices, Palo Alto, CA, USA) at 490 nm. The inhibition rate (%) was calculated using the following equation: [1-(A490/A490 control)] ×100%. The IC_{50} values were calculated from the inhibition curves in two independent experiments.

The activity of (*R*)-**21c**, at a concentration of 100 nM using an ATP concentration of 10 μM, was screened against a panel of other 43 human protein kinases by Eurofins using the Eurofins Kinase Profiler Selectivity Testing Service.

Cell culture

The human lung cancer cell line NCI-H1581, human acute myelogenous leukemia cancer cell line KG-1, and human gastric cancer cell line SNU-16 were purchased from American Type Culture Collection (ATCC, Manassas, VA, USA); human bladder cancer cell line RT112 was purchased from

DSMZ-German collection of microorganisms and cell cultures. All the cell lines were routinely maintained in media according to the suppliers' recommendations.

Cell proliferation assay

Cells were seeded in 96-well cell culture plates. On the day when seeding, the cells were exposed to various concentrations of compounds and further cultured for 72 h at 37 °C. Cell proliferation was then determined using Cell Counts Kit-8 (CCK8,) or the thiazolyl blue tetrazolium bromide (MTT, from Sigma-Aldrich, St.Louis, MO, USA) assay. The IC_{50} values were calculated by concentration-response curve fitting using the four-parameter method.

Statistical analysis

Data from the *in vitro* assays are presented as the mean ± SD. The statistical difference between multiple treatments and controls was analyzed using Student's *t* test. $P<0.05$ versus control group was considered statistically significant.

Pharmacokinetic parameters obtained in rats.

Compound (*R*)-**21c** or (*R*)-**22** was administrated to male Sprague-Dawley (SD) rats (n = 3): either as a 1 mg/kg intravenous in 10% DMSO + 90% (10% HP-β-CD in PBS), or orally by gavage as a suspension in 0.5% CMC-Na at a 5 mg/kg dose. Blood samples were collected at 0.08, 0.25, 0.5, 1, 1.5, 2, 4, 8, and 24 h time points following intravenous dosing and at 0.25, 0.5, 1, 1.5, 2, 4, 6, 8, and 24 h following oral dosing. The blood samples were placed on wet ice, and serum was collected after centrifugation. Serum samples were frozen stored at −80 °C. The serum samples were analyzed utilizing HPLC-coupled tandem mass spectrometry (LC-MS/MS).

Western blot analysis

KG-1 cell and SNU-16 cell were treated with the indicated dose of (*R*)-**21c** for 2 h, and then lysed in 1×sodium dodecyl sulfate (SDS) sample buffer. The cell lysates were subsequently resolved by 10% SDS-PAGE and transferred to nitrocellulose membranes. The membranes were probed with the appropriate primary antibodies [phospho-FGFR1, FGFR1, phospho-FGFR2, FGFR2, phospho-ERK, ERK, PLCγ (all from Cell Signaling Technology, Beverly, MA, USA), phospho-PLCγ, GAPDH (KangChen Biotech, Shanghai, China)] and then with horseradish peroxidase-conjugated anti-rabbit or anti-mouse IgG. The immunoreactive proteins were detected using an enhanced chemilluminescense detection reagent (Thermo Fisher Scientific, Rockford, IL, USA).

***In vivo* antitumor activity studies**

Female nude mice (4−6 weeks) were housed at five or six mice per cage in a specific pathogen free room with a 12 h light/dark schedule at 25 ± 1 °C; the animals were fed an autoclaved chow diet and water ad libitum. All animal experiments were performed according to the institutional ethical guidelines on animal care and approved by the Institute Animal Care and Use Committee at Shanghai Institute of Materia Medica (approval number: 2014-03-DJ-13).

NCI-H1581 cells at a density of 5×10^6 were first implanted subcutaneously into the right flank of each mouse and then allowed to grow to 700–800 mm^3, which was defined as a well-developed tumor. The well-developed tumors were cut into 1.5 mm^3 fragments and transplanted s.c. into the right flank of nude mice using a tracer. When the tumor volume reached 115 mm^3, the mice were randomly assigned into control and treatment groups. The control groups were given vehicle alone, and the treatment groups received (*R*)-**21c** at the indicated doses via oral administration once daily for 21 days. Compound **5** was a positive drug. The sizes of the tumors were measured twice per week using micro calipers. The tumor

volume (TV) was calculated as follows: TV = (length × width^2)/2. The tumor volume shown was obtained on the indicated days as the median tumor volume ± SEM for indicated groups of mice. The relative tumor volume (RTV) values were measured on the final day of the study for the drug-treated mice compared with the vehicle-treated mice and were calculated as RTV = V_t/V_0, while V_0 is the tumor volume at day 0, V_t is the tumor volume measured each time point. The percentage of tumor growth inhibition (TGI) values were also measured. Significant differences between the treated versus the control groups ($P \leq 0.05$) were determined using Student's t test.

Molecular Modeling

X-ray protein structure of FGFR1 (PDB ID: 3WJ6[24]) obtained in Protein Data Bank[43] was prepared with Protein Preparation Wizard panel as implemented in Maestro 9.0.[44] Both bond orders and hydrogen atoms were assigned and water molecules were removed. Hydrogen bond assignment and Impref minimization were performed subsequently. The size of box was set to 15Å×15Å×15Å centered in native ligand. Molecular docking simulations were conducted using Glide 5.5[45] with extra precision (Glide XP) mode.[46] Both the native ligand and the indicated compounds were built using 2D Sketcher and were prepared with LigPrep[47] with OPLS2005 forcefield,[48] generating possible states at pH 7.0 ± 2.0 using Epik 2.0 module.[49-50] Prior to docking the indicated compound, a redocking run was performed to evaluate the docking performance of Glide XP mode. Glide extra precision mode (Glide XP)[46] was successful in reproducing the binding mode of native ligand with a RMSD vale of 1.19 Å. Figure 3, 5, and 9 were generated with PyMOL Version 1.7.0.[51]

ASSOCIATED CONTENT

Supporting Information. Synthesis of intermediates **30**–**31**; analytical data for compounds **24**–**27**, **32**–**33**, **40**, (*S*)-**21c**, (*R*)-**22**, and (*S*)-**22**; supplementary kinase inhibition profile of (*R*)-**21c**; HPLC

analysis of all target compounds can be found. This material is available free of charge via the Internet at http://pubs.acs.org.

AUTHOR INFORMATION

Corresponding Authors

*J.A.: e-mail: jai@simm.ac.cn, phone: +86-21-50806600 ext. 2413;

*M.G.: e-mail: mygeng@simm.ac.cn, phone: +86-21-50806072;

*W.D.: email: whduan@simm.ac.cn, phone: +86-21-50806032.

Author Contributions

[#]These authors contributed equally.

Notes

The authors declared no competing financial interest.

ACKNOWLEDGMENTS

We thank the National Natural Science Foundation of China (81273365, 81573271, 91229205, 81473243, and 81321092), National Science & Technology Major Project ‘‘Key New Drug Creation and Manufacturing Program’’ (2014ZX09304002-008-001 and 2012ZX09301001-007), the Funding of Shanghai Institute of Materia Medica (CASIMM0120152005 and CASIMM01d20151011), and Chinese Academy of Sciences ‘Strategic Priority Research Program’ (XDA12020303) for their financial support. SA-SIBS Scholarship Program is also gratefully acknowledged.

ABBREVIATIONS USED

DCC, *N*,*N*’-dicyclohexylcarbodiimide; DDQ, 2,3-dichloro-5,6-dicyano-1,4-benzoquinone; DIAD, diisopropyl azodicarboxylate; DIPEA, *N*,*N*-diisopropylethylamine; DMAP, 4-dimethylaminopyridine; DMF, *N*,*N*-dimethylformamide; LDA, lithium diisopropylamide.

REFERENCES

(1) Touat, M.; Ileana, E.; Postel-Vinay, S.; Andre, F.; Soria, J. C. Targeting FGFR signaling in cancer. *Clin. Cancer Res.* **2015**, *21*, 2684–2694.

(2) Kelleher, F. C.; O'Sullivan, H.; Smyth, E.; McDermott, R.; Viterbo, A. Fibroblast growth factor receptors, developmental corruption and malignant disease. *Carcinogenesis* **2013**, *34*, 2198–2205.

(3) Weiss, J.; Sos, M. L.; Seidel, D.; Peifer, M.; Zander, T.; Heuckmann, J. M.; Ullrich, R. T.; Menon, R.; Maier, S.; Soltermann, A.; Moch, H.; Wagener, P.; Fischer, F.; Heynck, S.; Koker, M.; Schottle, J.; Leenders, F.; Gabler, F.; Dabow, I.; Querings, S.; Heukamp, L. C.; Balke-Want, H.; Ansen, S.; Rauh, D.; Baessmann, I.; Altmuller, J.; Wainer, Z.; Conron, M.; Wright, G.; Russell, P.; Solomon, B.; Brambilla, E.; Brambilla, C.; Lorimier, P.; Sollberg, S.; Brustugun, O. T.; Engel-Riedel, W.; Ludwig, C.; Petersen, I.; Sanger, J.; Clement, J.; Groen, H.; Timens, W.; Sietsma, H.; Thunnissen, E.; Smit, E.; Heideman, D.; Cappuzzo, F.; Ligorio, C.; Damiani, S.; Hallek, M.; Beroukhim, R.; Pao, W.; Klebl, B.; Baumann, M.; Buettner, R.; Ernestus, K.; Stoelben, E.; Wolf, J.; Nurnberg, P.; Perner, S.; Thomas, R. K. Frequent and focal FGFR1amplification associates with therapeutically tractable FGFR1 dependency in squamous cell lung cancer. *Sci. Transl. Med.* **2010**, *2*, 62ra93.

(4) Tomiguchi, M.; Yamamoto, Y.; Yamamoto-Ibusuki, M.; Goto-Yamaguchi, L.; Fujiki, Y.; Fujiwara, S.; Sueta, A.; Hayashi, M.; Takeshita, T.; Inao, T.; Iwase, H. FGFR1 protein expression is associated with prognosis in ER-positive/HER2-negative primary breast cancer. *Cancer Sci.* **2016**. [Online early access]. DOI: 10.1111/cas.12897. Published Online: January 23, 2016.

(5) Shoji, H.; Yamada, Y.; Okita, N.; Takashima, A.; Honma, Y.; Iwasa, S.; Kato, K.; Hamaguchi, T.; Shimada, Y. Amplification of FGFR2 gene in patients with advanced gastric cancer receiving chemotherapy: prevalence and prognostic significance. *Anticancer Res.* **2015**, *35*, 5055–5061.

(6) Neuzillet, Y.; van Rhijn, B. W.; Prigoda, N. L.; Bapat, B.; Liu, L.; Bostrom, P. J.; Fleshner, N. E.; Gallie, B. L.; Zlotta, A. R.; Jewett, M. A.; van der Kwast, T. H. FGFR3 mutations, but not FGFR3 expression and FGFR3 copy-number variations, are associated with favourable non-muscle invasive bladder cancer. *Virchows Arch.* **2014**, *465*, 207–213.

(7) Taylor, J. G. 6th; Cheuk, A. T.; Tsang, P. S.; Chung, J. Y.; Song, Y. K.; Desai, K.; Yu, Y.; Chen, Q. R.; Shah, K.; Youngblood, V.; Fang, J.; Kim, S. Y.; Yeung, C.; Helman, L. J.; Mendoza, A.; Ngo, V.; Staudt, L. M.; Wei, J. S.; Khanna, C.; Catchpoole, D.; Qualman, S. J.; Hewitt, S. M.; Merlino, G.; Chanock, S. J.; Khan, J. Identification of FGFR4-activating mutations in human rhabdomyosarcomas that promote metastasis in xenotransplanted models. *J. Clin. Invest.* **2009**, *119*, 3395–3407.

(8) Gauglhofer, C.; Paur, J.; Schrottmaier, W. C.; Wingelhofer, B.; Huber, D.; Naegelen, I.; Pirker, C.; Mohr, T.; Heinzle, C.; Holzmann, K.; Marian, B.; Schulte-Hermann, R.; Berger, W.; Krupitza, G.; Grusch, M.; Grasl-Kraupp, B. Fibroblast growth factor receptor 4: a putative key driver for the aggressive phenotype of hepatocellular carcinoma. *Carcinogenesis* **2014**, *35*, 2331–2338.

(9) Kim, B.; Wang, S.; Lee, J. M.; Jeong, Y.; Ahn, T.; Son, D. S.; Park, H. W.; Yoo, H. S.; Song, Y. J.; Lee, E.; Oh, Y. M.; Lee, S. B.; Choi, J.; Murray, J. C.; Zhou, Y.; Song, P. H.; Kim, K. A.; Weiner, L. M. Synthetic lethal screening reveals FGFR as one of the combinatorial targets to overcome resistance to Met-targeted therapy. *Oncogene* **2015**, *34*, 1083–1093.

(10) Saito, S.; Morishima, K.; Ui, T.; Hoshino, H.; Matsubara, D.; Ishikawa, S.; Aburatani, H.; Fukayama, M.; Hosoya, Y.; Sata, N.; Lefor, A. K.; Yasuda, Y.; Niki, T. The role of HGF/MET and FGF/FGFR in fibroblast-derived growth stimulation and lapatinib-resistance of esophageal squamous cell carcinoma. *BMC Cancer* **2015**, *15*, 82.

(11) Turner, N.; Pearson, A.; Sharpe, R.; Lambros, M.; Geyer, F.; Lopez-Garcia, M. A.; Natrajan, R.; Marchio, C.; Iorns, E.; Mackay, A.; Gillett, C.; Grigoriadis, A.; Tutt, A.; Reis-Filho, J. S.; Ashworth, A. FGFR1 amplification drives endocrine therapy resistance and is a therapeutic target in breast cancer. *Cancer Res.* **2010**, *70*, 2085–2094.

(12) Renhowe, P. A.; Pecchi, S.; Shafer, C. M.; Machajewski, T. D.; Jazan, E. M.; Taylor, C.; Antonios-McCrea, W.; McBride, C. M.; Frazier, K.; Wiesmann, M.; Lapointe, G. R.; Feucht, P. H.; Warne, R. L.; Heise, C. C.; Menezes, D.; Aardalen, K.; Ye, H.; He, M.; Le, V.; Vora, J.; Jansen, J. M.; Wernette-Hammond, M. E.; Harris, A. L. Design, structure-activity relationships and *in vivo* characterization of 4-amino-3-benzimidazol-2-ylhydroquinolin-2-ones: a novel class of receptor tyrosine kinase inhibitors. *J. Med. Chem.* **2009**, *52*, 278–292.

(13) Roth, G. J.; Heckel, A.; Colbatzky, F.; Handschuh, S.; Kley, J.; Lehmann-Lintz, T.; Lotz, R.; Tontsch-Grunt, U.; Walter, R.; Hilberg, F. Design, synthesis, and evaluation of indolinones as triple angiokinase inhibitors and the discovery of a highly specific 6-methoxycarbonyl-substituted indolinone (BIBF 1120). *J. Med. Chem.* **2009**, *52*, 4466–4480.

(14) Wedge, S. R.; Kendrew, J.; Hennequin, L. F.; Valentine, P. J.; Barry, S. T.; Brave, S. R.; Smith, N. R.; James, N. H.; Dukes, M.; Curwen, J. O.; Chester, R.; Jackson, J. A.; Boffey, S. J.; Kilburn, L. L.; Barnett, S.; Richmond, G. H.; Wadsworth, P. F.; Walker, M.; Bigley, A. L.; Taylor, S. T.; Cooper, L.; Beck, S.; Jurgensmeier, J. M.; Ogilvie, D. J. AZD2171: a highly potent, orally bioavailable, vascular endothelial growth factor receptor-2 tyrosine kinase inhibitor for the treatment of cancer. *Cancer Res.* **2005**, *65*, 4389–4400.

(15) Izzedine, H.; Buhaescu, I.; Rixe, O.; Deray, G. Sunitinib malate. *Cancer Chemother. Pharmacol.* **2007**, *60*, 357–364.

(16) Ahmad, T.; Eisen, T. Kinase inhibition with BAY 43-9006 in renal cell carcinoma. *Clin. Cancer Res.* **2004**, *10*, 6388S–6392S.

(17) Harris, P. A.; Boloor, A.; Cheung, M.; Kumar, R.; Crosby, R. M.; Davis-Ward, R. G.; Epperly, A. H.; Hinkle, K. W.; Hunter, R. N. 3rd; Johnson, J. H.; Knick, V. B.; Laudeman, C. P.; Luttrell, D. K.; Mook, R. A.; Nolte, R. T.; Rudolph, S. K.; Szewczyk, J. R.; Truesdale, A. T.; Veal, J. M.; Wang, L.; Stafford, J. A. Discovery of 5-[[4-[(2,3-dimethyl-2*H*-indazol-6-yl)methylamino]-2-pyrimidinyl]amino]-2-methyl-benzenesulfonamide (Pazopanib), a novel and potent vascular endothelial growth factor receptor inhibitor. *J. Med. Chem.* **2008**, *51*, 4632–4640.

(18) Wedge S. R.; Ogilvie D. J.; Dukes M.; Kendrew J.; Chester R.; Jackson J. A.; Boffey S. J.; Valentine P. J.; Curwen J. O.; Musgrove H. L.; Graham G. A.; Hughes G. D.; Thomas A. P.; Stokes E. S. E.; Curry B.; Richmond G. H. P.; Wadsworth P. F.; Bigley A. L.; Hennequin L. F. ZD6474 inhibits vascular endothelial growth factor signaling, angiogenesis, and tumor growth following oral administration. *Cancer Res.* **2002**, *62*, 4645–4655.

(19) Cohen, R. B.; Oudard, S. Antiangiogenic therapy for advanced renal cell carcinoma: management of treatment-related toxicities. *Invest. New Drugs* **2012**, *30*, 2066–2079.

(20) Herbst, R. S. Toxicities of antiangiogenic therapy in non-small-cell lung cancer. *Clin. Lung Cancer* **2006**, *8*, S23–S30.

(21) Tuder, R. M.; Chacon, M.; Alger, L.; Wang, J.; Taraseviciene-Stewart, L.; Kasahara, Y.; Cool, C. D.; Bishop, A. E.; Geraci, M.; Semenza, G. L.; Yacoub, M.; Polak, J. M.; Voelkel, N. F. Expression of angiogenesis-related molecules in plexiform lesions in severe pulmonary hypertension: evidence for a process of disordered angiogenesis. *J. Pathol.* **2001**, *195*, 367–374.

(22) Guagnano, V.; Furet, P.; Spanka, C.; Bordas, V.; Le Douget, M.; Stamm, C.; Brueggen, J.; Jensen, M. R.; Schnell, C.; Schmid, H.; Wartmann, M.; Berghausen, J.; Drueckes, P.; Zimmerlin, A.; Bussiere, D.; Murray, J.; Graus Porta, D. Discovery of 3-(2,6-dichloro-3,5-dimethoxy-phenyl)-1-{6-[4-(4-ethyl-piperazin-1-yl)-phenylamino]-pyrimidin-4-yl}-1-methyl-urea (NVP-BGJ398), a potent and selective inhibitor of the fibroblast growth factor receptor family of receptor tyrosine kinase. *J. Med. Chem.* **2011**, *54*, 7066–7083.

(23) Gavine, P. R.; Mooney, L.; Kilgour, E.; Thomas, A. P.; Al-Kadhimi, K.; Beck, S.; Rooney, C.; Coleman, T.; Baker, D.; Mellor, M. J.; Brooks, A. N.; Klinowska, T. AZD4547: an orally bioavailable, potent, and selective inhibitor of the fibroblast growth factor receptor tyrosine kinase family. *Cancer Res.* **2012**, *72*, 2045–2056.

(24) Nakanishi, Y.; Akiyama, N.; Tsukaguchi, T.; Fujii, T.; Sakata, K.; Sase, H.; Isobe, T.; Morikami, K.; Shindoh, H.; Mio, T.; Ebiike, H.; Taka, N.; Aoki, Y.; Ishii, N. The fibroblast growth factor receptor genetic status as a potential predictor of the sensitivity to CH5183284/Debio 1347, a novel selective FGFR inhibitor. *Mol. Cancer Ther.* **2014**, *13*, 2547–2558.

(25) Zhao, G.; Li, W. Y.; Chen, D.; Henry, J. R.; Li, H. Y.; Chen, Z.; Zia-Ebrahimi, M.; Bloem, L.; Zhai, Y.; Huss, K.; Peng, S. B.; McCann, D. J. A novel, selective inhibitor of fibroblast growth factor receptors that shows a potent broad spectrum of antitumor activity in several tumor xenograft models. *Mol. Cancer. Ther.* **2011**, *10*, 2200–2210.

(26) Thompson, A. M.; Delaney, A. M.; Hamby, J. M.; Schroeder, M. C.; Spoon, T. A.; Crean, S. M.; Showalter, H. D.; Denny, W. A. Synthesis and structure-activity relationships of soluble 7-substituted 3-(3,5-dimethoxyphenyl)-1,6-naphthyridin-2-amines and related ureas as dual inhibitors of the fibroblast

growth factor receptor-1 and vascular endothelial growth factor receptor-2 tyrosine kinases. *J. Med. Chem.* **2005**, *48*, 4628–4653.

(27) Mohammadi, M.; Froum, S.; Hamby, J. M.; Schroeder, M. C.; Panek, R. L.; Lu, G. H.; Eliseenkova, A. V.; Green, D.; Schlessinger, J.; Hubbard, S. R. Crystal structure of an angiogenesis inhibitor bound to the FGF receptor tyrosine kinase domain. *EMBO J.* **1998**, *17*, 5896–5904.

(28) Grygielewicz, P.; Dymek, B.; Bujak, A.; Gunerka, P.; Stanczak, A.; Lamparska-Przybysz, M.; Wieczorek, M.; Dzwonek, K.; Zdzalik, D. Epithelial-mesenchymal transition confers resistance to selective FGFR inhibitors in SNU-16 gastric cancer cells. *Gastric Cancer* **2016**, *19*, 53–62.

(29) Javidi-Sharifi, N.; Traer, E.; Martinez, J.; Gupta, A.; Taguchi, T.; Dunlap, J.; Heinrich, M. C.; Corless, C. L.; Rubin, B. P.; Druker, B. J.; Tyner, J. W. Crosstalk between KIT and FGFR3 promotes gastrointestinal stromal tumor cell growth and drug resistance. *Cancer Res.* **2015**, *75*, 880–891.

(30) Byron, S. A.; Chen, H.; Wortmann, A.; Loch, D.; Gartside, M. G.; Dehkhoda, F.; Blais, S. P.; Neubert, T. A.; Mohammadi, M.; Pollock, P. M. The N550K/H mutations in FGFR2 confer differential resistance to PD173074, dovitinib, and ponatinib ATP-competitive inhibitors. *Neoplasia* **2013**, *15*, 975–988.

(31) McBride, C. M.; Renhowe, P. A.; Heise, C.; Jansen, J. M.; Lapointe, G.; Ma, S.; Pineda, R.; Vora, J.; Wiesmann, M.; Shafer, C. M. Design and structure-activity relationship of 3-benzimidazol-2-yl-1*H*-indazoles as inhibitors of receptor tyrosine kinases. *Bioorg. Med. Chem. Lett.* **2006**, *16*, 3595–3599.

(32) Cui, J. J.; Tran-Dube, M.; Shen, H.; Nambu, M.; Kung, P. P.; Pairish, M.; Jia, L.; Meng, J.; Funk, L.; Botrous, I.; McTigue, M.; Grodsky, N.; Ryan, K.; Padrique, E.; Alton, G.; Timofeevski, S.; Yamazaki, S.; Li, Q.; Zou, H.; Christensen, J.; Mroczkowski, B.; Bender, S.; Kania, R. S.; Edwards, M.

P. Structure based drug design of crizotinib (PF-02341066), a potent and selective dual inhibitor of mesenchymal-epithelial transition factor (c-MET) kinase and anaplastic lymphoma kinase (ALK). *J. Med. Chem.* **2011**, *54*, 6342–6363.

(33) Ho, H. K.; Pok, S.; Streit, S.; Ruhe, J. E.; Hart, S.; Lim, K. S.; Loo, H. L.; Aung, M. O.; Lim, S. G.; Ullrich, A. Fibroblast growth factor receptor 4 regulates proliferation, anti-apoptosis and alpha-fetoprotein secretion during hepatocellular carcinoma progression and represents a potential target for therapeutic intervention. *J. Hepatol.* **2009**, *50*, 118–127.

(34) Buchi, G.; Lee, G. C.; Yang, D.; Tannenbaum, S. R. Direct acting, highly mutagenic, α-hydroxy *N*-nitrosamines from 4-chloroindoles. *J. Am. Chem. Soc.* **1986**, *108*, 4115–4119.

(35) Mizuta, M.; Seio, K.; Miyata, K.; Sekine, M. Fluorescent pyrimidopyrimidoindole nucleosides: control of photophysical characterizations by substituent effects. *J. Org. Chem.* **2007**, *72*, 5046–5055.

(36) Chen, D. H.; Li, H. Y.; Zhao, G. S. Vinyl indazolyl compounds. Patent WO2010129509, 2010.

(37) Ramachandran, S.; Hameed, P. S.; Srivastava, A.; Shanbhag, G.; Morayya, S.; Rautela, N.; Awasthy, D.; Kavanagh, S.; Bharath, S.; Reddy, J.; Panduga, V.; Prabhakar, K. R.; Saralaya, R.; Nanduri, R.; Raichurkar, A.; Menasinakai, S.; Achar, V.; Jimenez-Diaz, M. B.; Martinez, M. S.; Angulo-Barturen, I.; Ferrer, S.; Sanz, L. M.; Gamo, F. J.; Duffy, S.; Avery, V. M.; Waterson, D.; Lee, M. C. S.; Coburn-Flynn, O.; Fidock, D. A.; Iyer, P. S.; Narayanan, S.; Hosagrahara, V.; Sambandamurthy, V. K. *N*-aryl-2-aminobenzimidazoles: novel, efficacious, antimalarial lead compounds. *J. Med. Chem.* **2014**, *57*, 6642–6652.

(38) Young, J. R.; Huang, S. X.; Walsh, T. F.; Wyvratt, M. J.; Yang, Y. T.; Yudkovitz, J. B.; Cui, J.; Mount, G. R.; Ren, R. N.; Wu, T. J.; Shen, X.; Lyons, K. A.; Mao, A. H.; Carlin, J. R.; Karanam, B. V.;

Vincent, S. H.; Cheng, K.; Goulet, M. T. 2-Arylindoles as gonadotropin releasing hormone (GnRH) antagonists: optimization of the tryptamine side chain. *Bioorg. Med. Chem. Lett.* **2002**, *12*, 827–832.

(39) Chinchilla, R.; Nájera, C.; Yus, M.; Heumann, A. Kinetic resolution of racemic alcohols with chiral carboxylic acids and dicyclohexylcarbodiimide. *Tetrahedron: Asymmetry* **1990**, *1*, 851–854.

(40) Foloppe, N.; Fisher, L. M.; Francis, G.; Howes, R.; Kierstan, P.; Potter, A. Identification of a buried pocket for potent and selective inhibition of Chk1: prediction and verification. *Bioorg. Med. Chem.* **2006**, *14*, 1792–1804.

(41) Chang, J. B.; Zhao, K.; Pan, S. F. Synthesis of 2-arylbenzoxazoles via DDQ promoted oxidative cyclization of phenolic Schiff bases—a solution-phase strategy for library synthesis. *Tetrahedron Lett.* **2002**, *43*, 951–954.

(42) Moir, D. T.; Aiello, D.; Peet, N. P.; Williamms, J. D. Inhibitors of bacterial type III secretion system. Patent WO2010118046, 2010.

(43) Berman, H. M.; Westbrook, J.; Feng, Z.; Gilliland, G.; Bhat, T. N.; Weissig, H.; Shindyalov, I. N.; Bourne, P. E. The Protein Data Bank. *Nucleic Acids Res.* **2000**, *28*, 235–242.

(44) *Maestro*, version 9.0; Schrödinger, LLC: New York, NY, 2009.

(45) *Glide*, version 5.5; Schrödinger, LLC: New York, NY, 2009.

(46) Friesner, R. A.; Murphy, R. B.; Repasky, M. P.; Frye, L. L.; Greenwood, J. R.; Halgren, T. A.; Sanschagrin, P. C.; Mainz, D. T. Extra precision glide: docking and scoring incorporating a model of hydrophobic enclosure for protein−ligand complexes. *J. Med. Chem.* **2006**, *49*, 6177–6196.

(47) *LigPrep*, version 2.3; Schrödinger, LLC: New York, NY, 2009.

(48) Banks, J. L.; Beard, H. S.; Cao, Y.; Cho, A. E.; Damm, W.; Farid, R.; Felts, A. K.; Halgren, T. A.; Mainz, D. T.; Maple, J. R.; Murphy, R.; Philipp, D. M.; Repasky, M. P.; Zhang, L. Y.; Berne, B. J.; Friesner, R. A.; Gallicchio, E.; Levy, R. M. Integrated modeling program, applied chemical theory (IMPACT). *J. Comput. Chem.* **2005**, *26*, 1752–1780.

(49) *Epik*, version 2.0; Schrödinger, LLC: New York, NY, 2009.

(50) Shelley, J. C.; Cholleti, A.; Frye, L. L.; Greenwood, J. R.; Timlin, M. R.; Uchimaya, M. Epik: a software program for pK_a prediction and protonation state generation for drug-like molecules. *J. Comput. Aided Mol. Des.* **2007**, *21*, 681–691.

(51) *The PyMOL molecular graphics system*, version 1.7.0; Schrodinger, LLC: New York, NY, 2014.

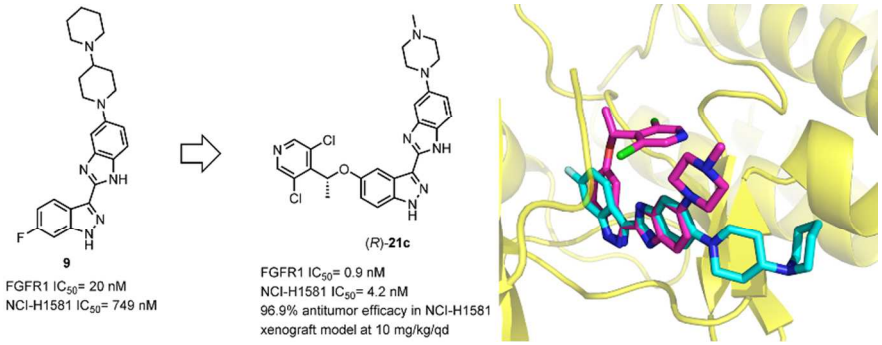

Table of Contents Graphic

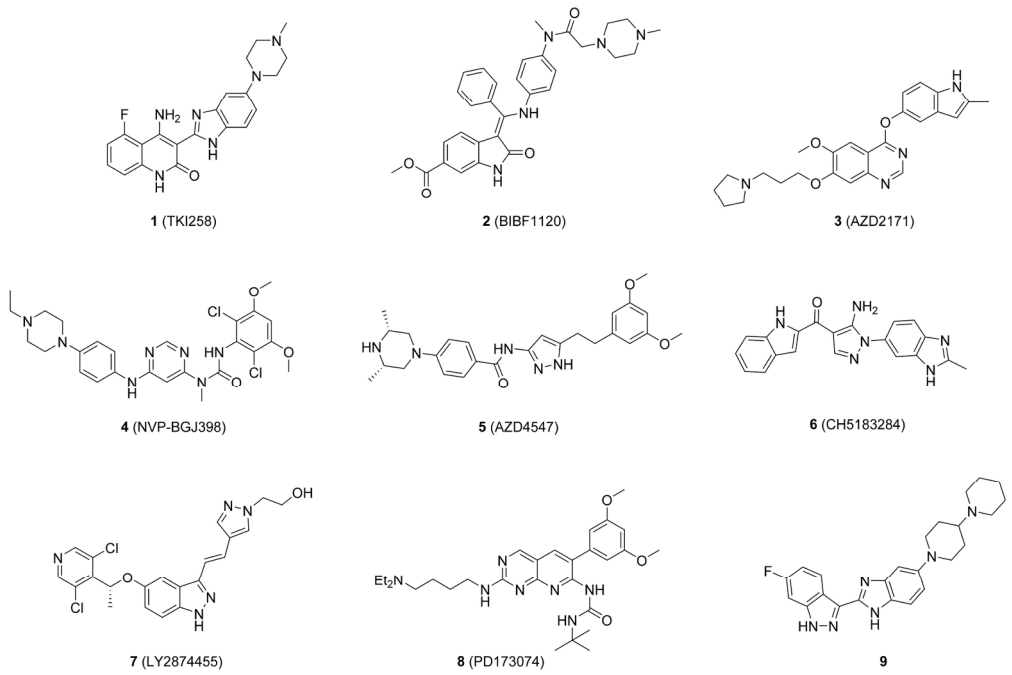

Figure 1. Structures of representative FGFR inhibitors.
86x58mm (600 x 600 DPI)

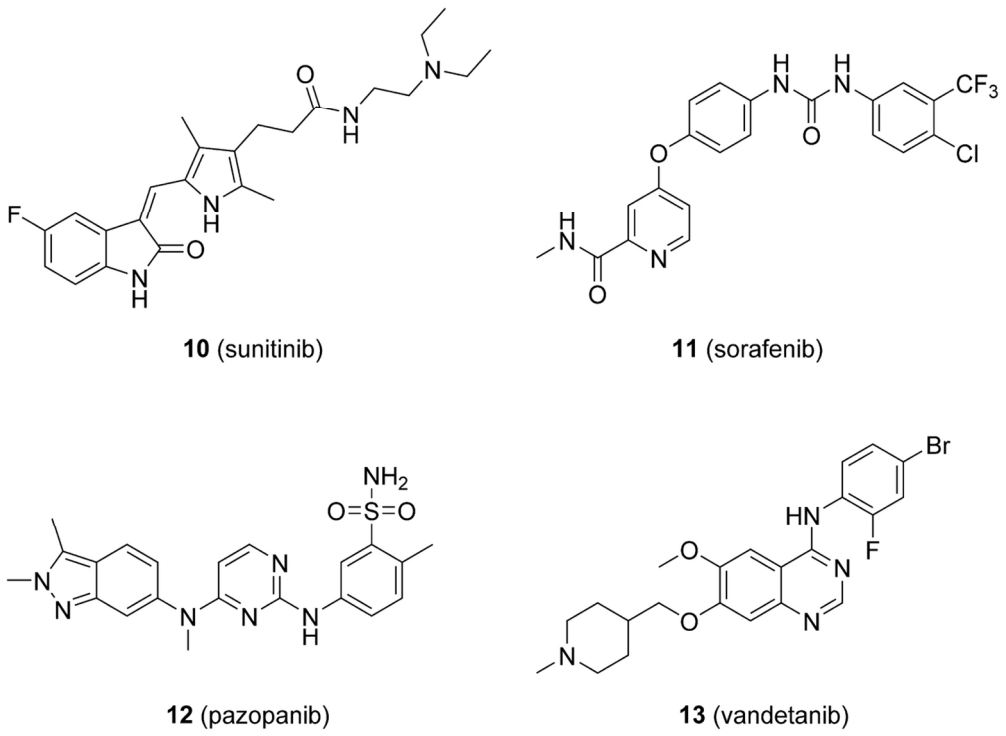

Figure 2. Structures of representative approved VEGFR2 inhibitors.
61x45mm (600 x 600 DPI)

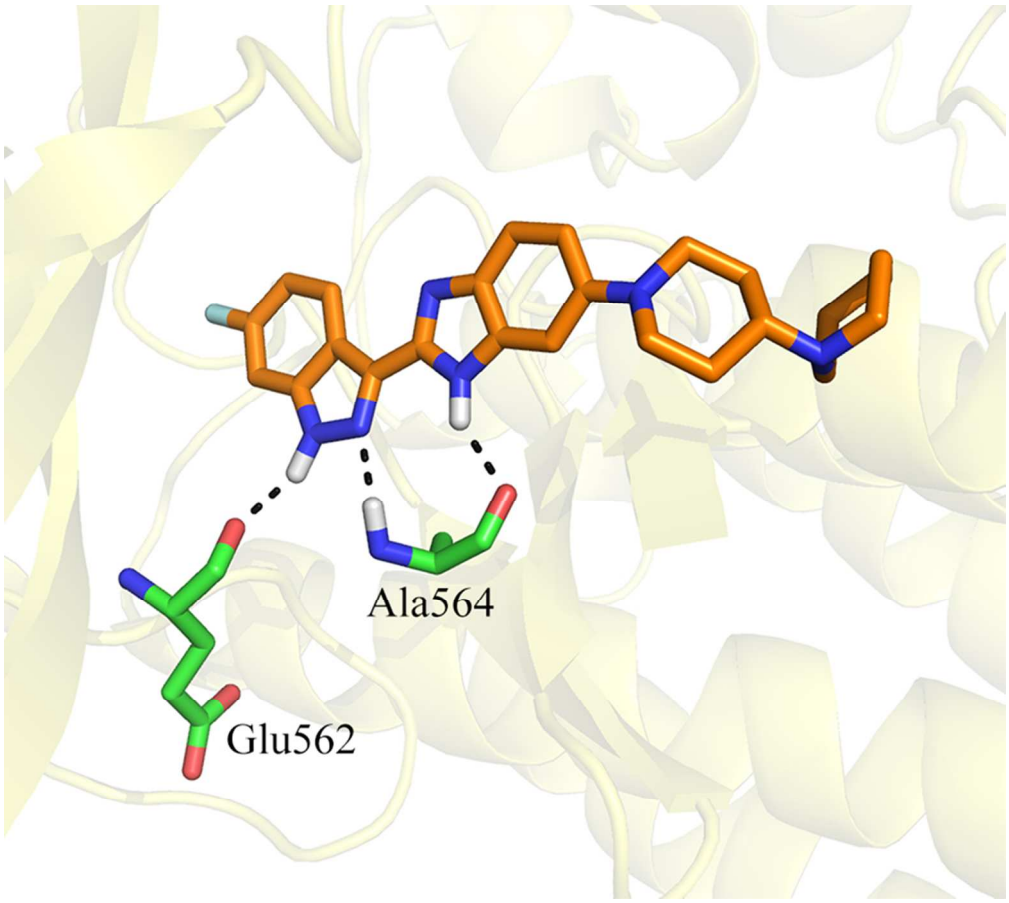

Figure 3. Proposed binding mode of compound **9** to FGFR1 kinase domain. The atoms of compound **9** are colored as follows: carbon orange, oxygen red, nitrogen blue, fluorine light blue, and hydrogen white. The docked protein structure of FGFR1 is shown in the cartoon and key residues are colored as follows: carbon green, oxygen red, nitrogen blue, and hydrogen white. The hydrogen bonds are colored in black.
84x75mm (300 x 300 DPI)

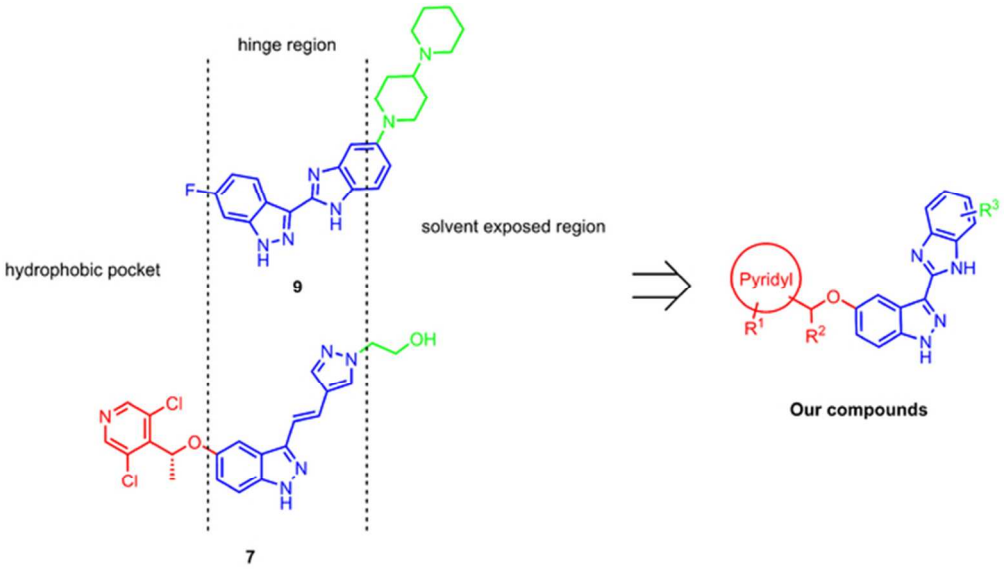

Figure 4. Design of our compounds.
56x32mm (300 x 300 DPI)

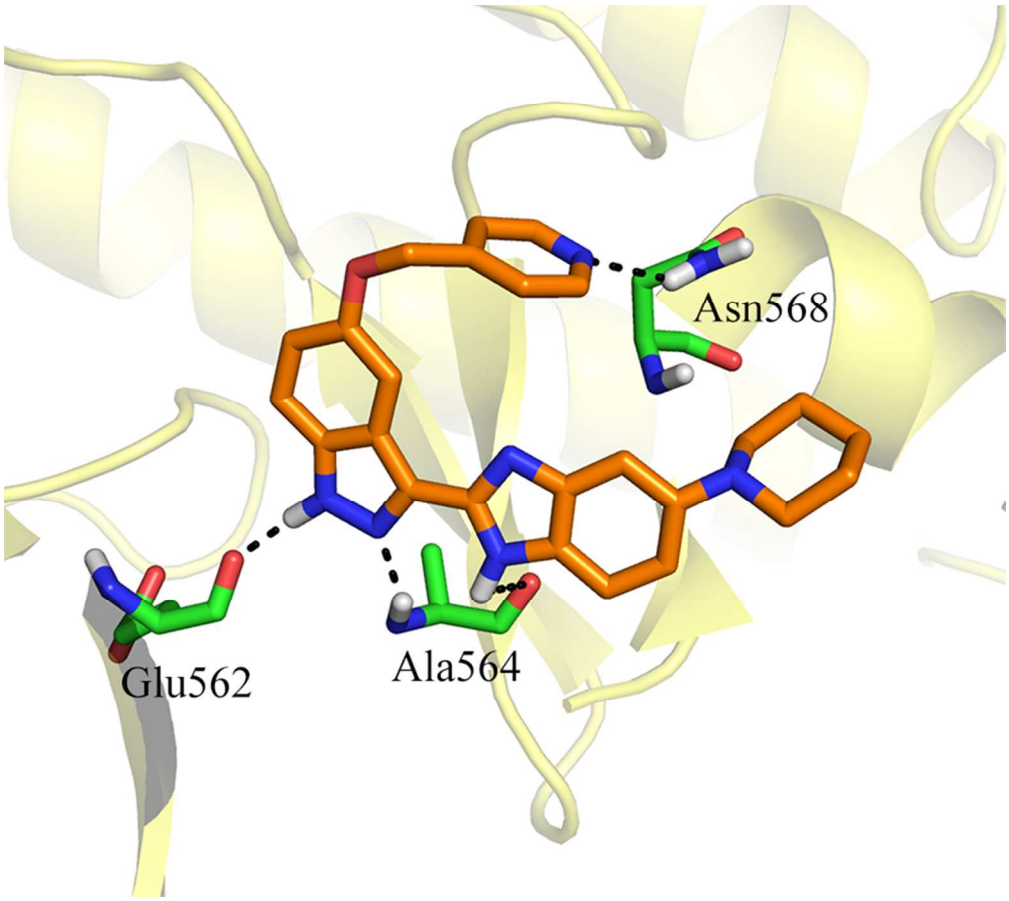

Figure 5. Proposed binding mode of compound **14a** to FGFR1 kinase domain. The atoms of compound **14a** are colored as follows: carbon orange, oxygen red, nitrogen blue, and hydrogen white. The docked protein structure of FGFR1 is shown in the cartoon and key residues are colored as follows: carbon green, oxygen red, nitrogen blue, and hydrogen white. The hydrogen bonds are colored in black.
84x75mm (300 x 300 DPI)

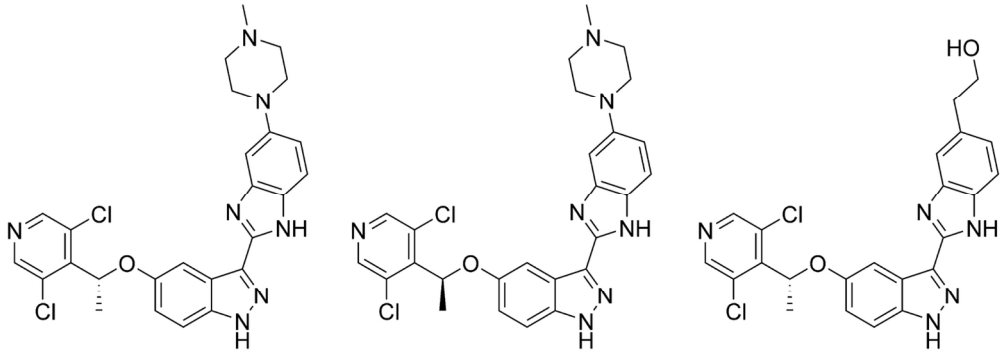

(*R*)-**21c** (*S*)-**21c** (*R*)-**22**

Compound	FGFR1 IC_{50} (nM)	NCI-H1581 IC_{50} (nM)
(*R*)-**21c**	0.9	4.2
(*S*)-**21c**	9.4	129.5
(*R*)-**22**	1.2	1.4
(*S*)-**22**	6.5	>100

Figure 6. Structures and activities of **21c** and **22**.
65x50mm (600 x 600 DPI)

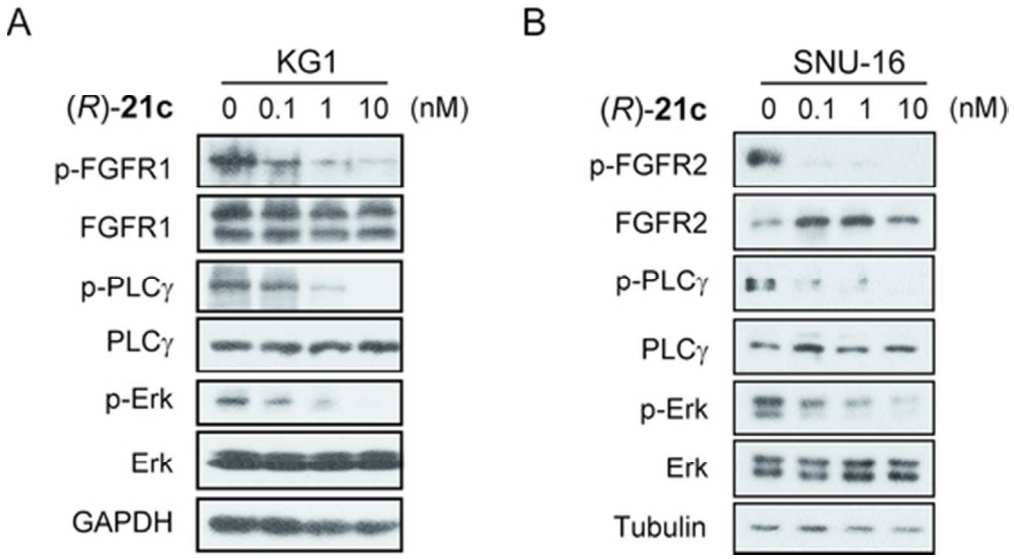

Figure 7. Compound (*R*)-**21c** effectively inhibits the phosphorylation of FGFR and the downstream effectors PLCγ and Erk in KG-1 and SNU-16 cells. KG1 (A) or SNU-16 (B) cells treated with (*R*)-**21c** for 2 h at the indicated concentrations were lysed and subjected to western blot analysis.
46x25mm (300 x 300 DPI)

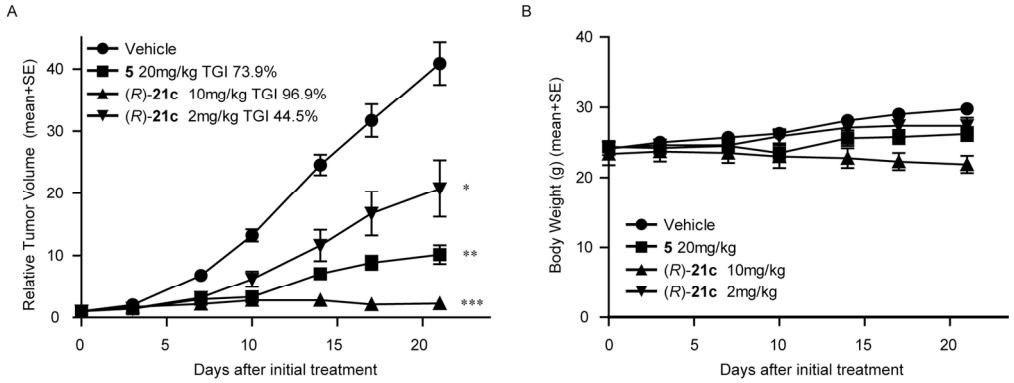

Figure 8. The inhibitory effect of (*R*)-**21c** on tumor growth in NCI-H1581 xenograft model. Compound (*R*)-**21c** was administered orally once daily for 21 days. (A) The percentage of tumor growth inhibition values (TGI) was measured on the final day of the study for the drug-treated mice compared with the vehicle control mice: (∗) $P < 0.05$, (∗∗) $P < 0.01$, (∗∗∗) $P < 0.001$, versus vehicle group, using Student's t test. Results are expressed as the mean ± SEM (n = 6 for inhibitor-treated group, n = 12 for vehicle control group). (B) Body weight measurements during the treatment.
75x28mm (600 x 600 DPI)

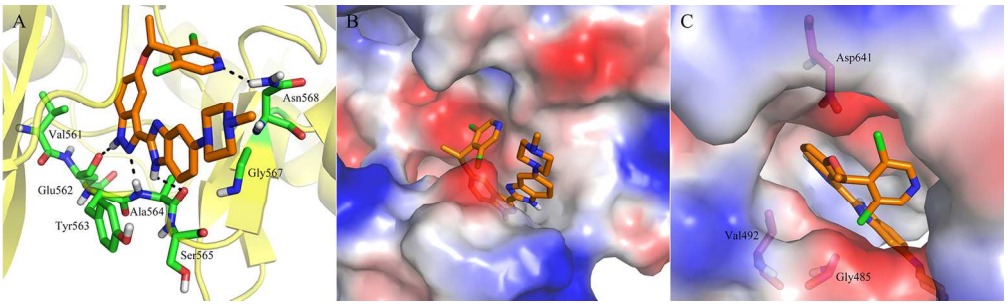

Figure 9. The proposed binding mode of (*R*)-**21c** with FGFR1. (A) The atoms of (*R*)-**21c** are colored as follows: carbon orange, oxygen red, nitrogen blue, chlorine green, and hydrogen white. The docked protein structure of FGFR1 is shown in the cartoon and key residues are colored as follows: carbon green, oxygen red, nitrogen blue, and hydrogen white. The hydrogen bonds are colored in black. (B) The docked protein structure of FGFR1 is shown in surface. The surfaces of Gly485 and Glu486 are omitted for clarity. (C) The *R*-methyl fit in a pocket surrounded by three residues (Asp641, Val492, and Glu485).
160x47mm (300 x 300 DPI)

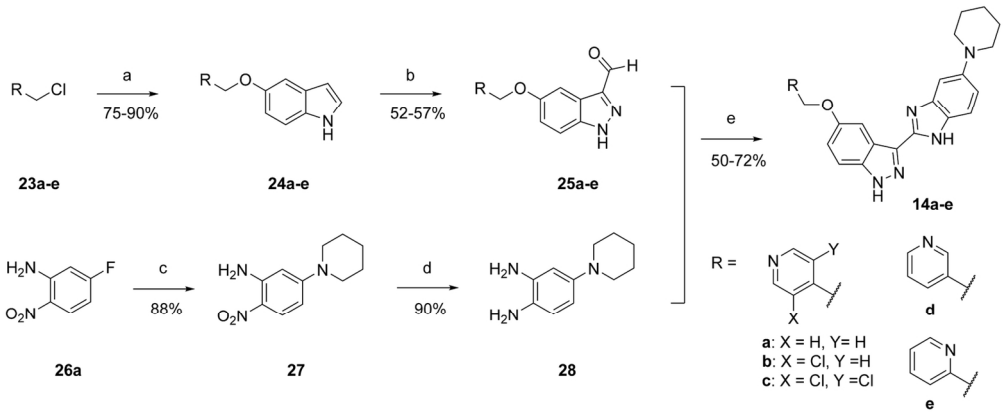

Scheme 1[a] [a]Reagents and conditions: (a) 5-hydroxyindole, Cs_2CO_3, DMF, 70 °C; (b) $NaNO_2$, HCl, H_2O/dioxane, 0 °C to rt; (c) Et_3N, piperidine, NMP, 120 °C; (d) H_2, 10% Pd/C, MeOH, rt; (e) S_8, DMF, 90 °C.
70x28mm (600 x 600 DPI)

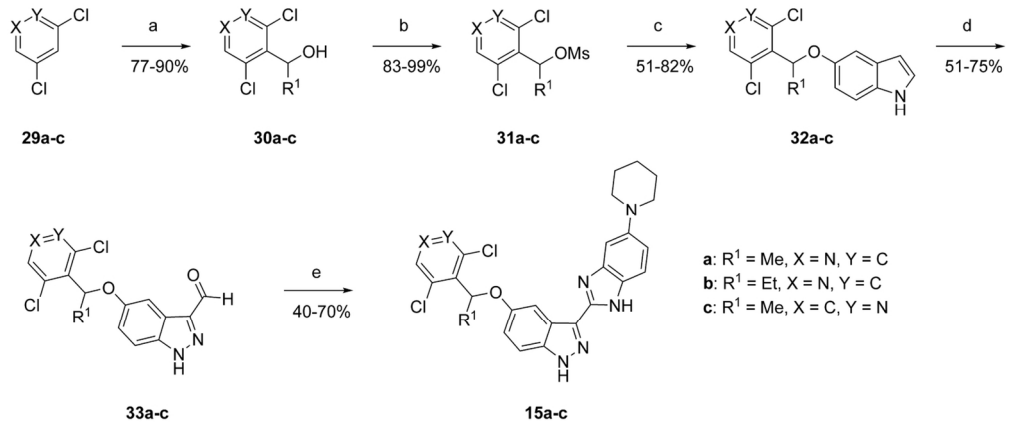

Scheme 2[a] [a]Reagents and conditions: (a) for **30a** and **30c**, LDA, acetaldhyde, THF, −78 °C; for **30b**, LDA, propionaldehyde, THF, −78 °C; (b) MsCl, Et_3N, CH_2Cl_2, 0 °C to rt; (c) 5-hydroxyindole, Cs_2CO_3, DMF, 70 °C; (d) $NaNO_2$, HCl, H_2O/dioxane, 0 °C to rt; (e) **28**, S_8, DMF, 90 °C.
63x26mm (600 x 600 DPI)

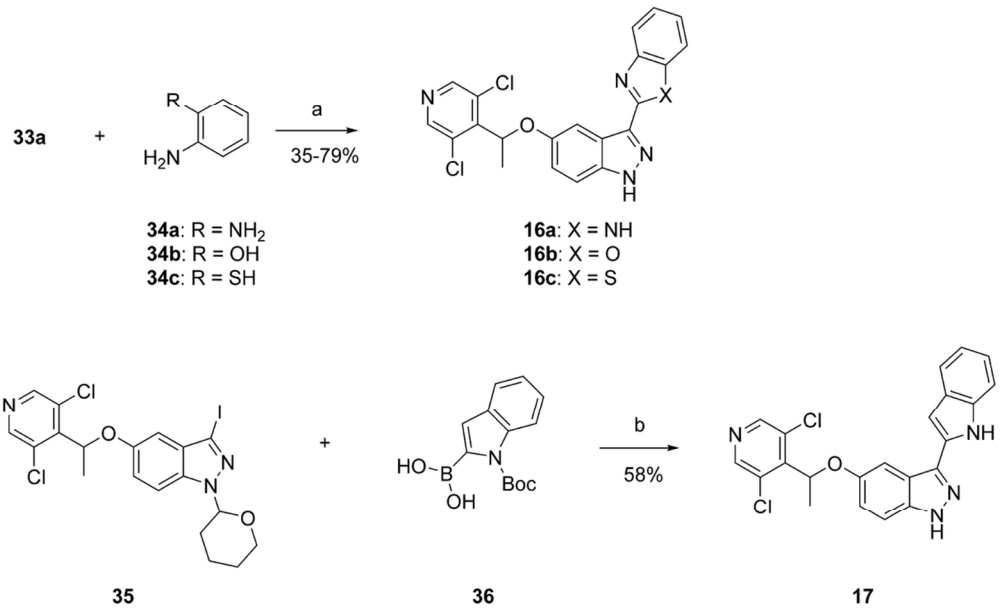

Scheme 3[a] [a]Reagents and conditions: (a) for **16a** and **16c**, S_8, DMF, 90 °C; for **16b**, (i) DMF, 90 °C; (ii) DDQ, $CHCl_3$, reflux; (b) (i) Cs_2CO_3, $Pd(dppf)_2Cl_2$, dioxane, 90 °C; (ii) 4 N HCl in MeOH.
51x31mm (600 x 600 DPI)

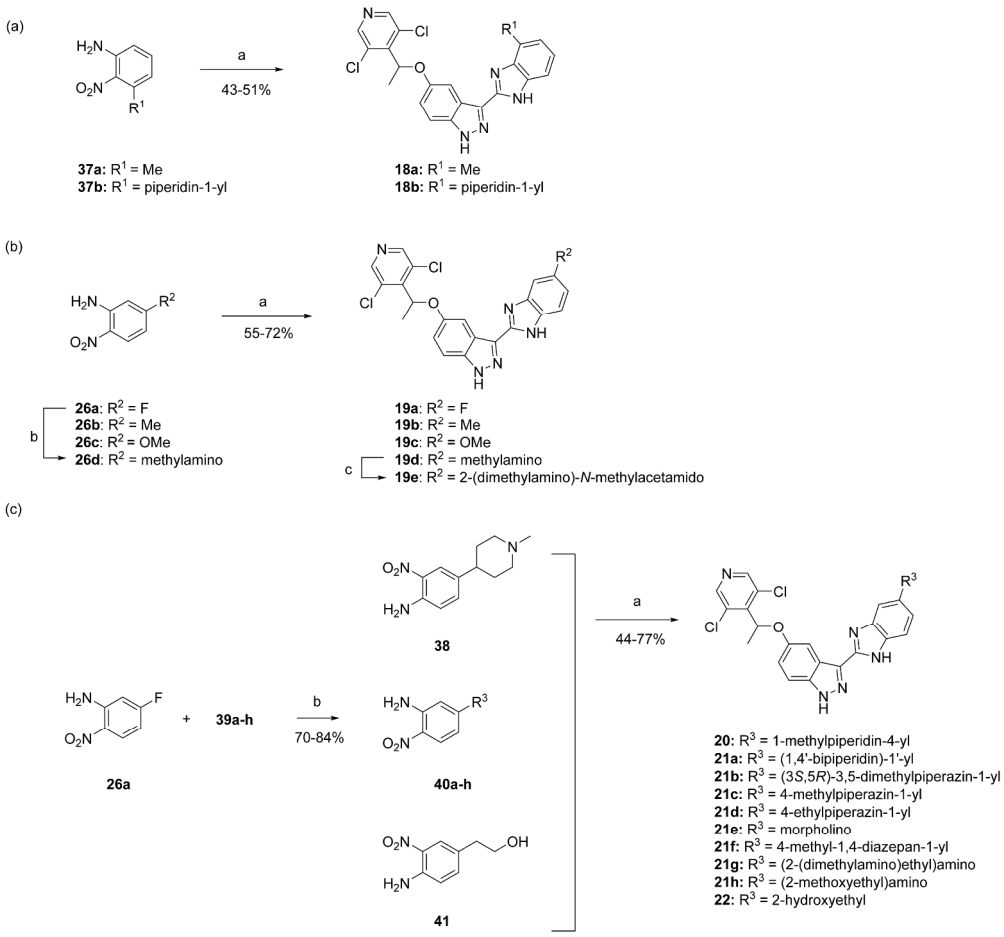

Scheme 4[a] [a]Reagents and conditions: (a) (i) H_2, 10% Pd/C, MeOH, rt; (ii) **33a**, S_8, DMF, 90 °C; (b) for **26d**, methylammonium chloride, DIPEA, NMP, 140 °C; for **40**, DIPEA, NMP, 120 °C; (c) (i) 2-bromoacetyl chloride, CH_2Cl_2, rt; (ii) dimethylamine, THF, rt.
121x112mm (600 x 600 DPI)

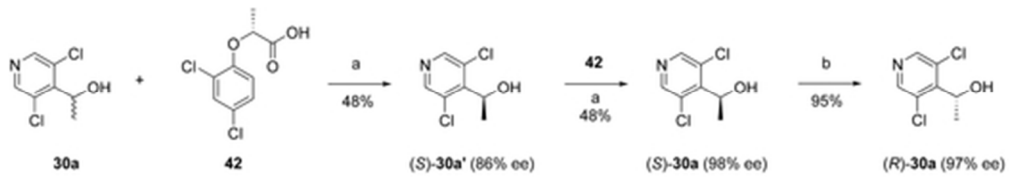

Scheme 5[a] *a*Reagents and conditions: (a) (i) DCC, 4-DMAP, toluene, 0 oC; (ii) NaOH, H_2O, EtOH, rt; (b) (i) HOAc, DIAD, PPh_3, THF, 0 oC to rt; (ii) NaOH, H_2O, EtOH, rt.

22x3mm (600 x 600 DPI)

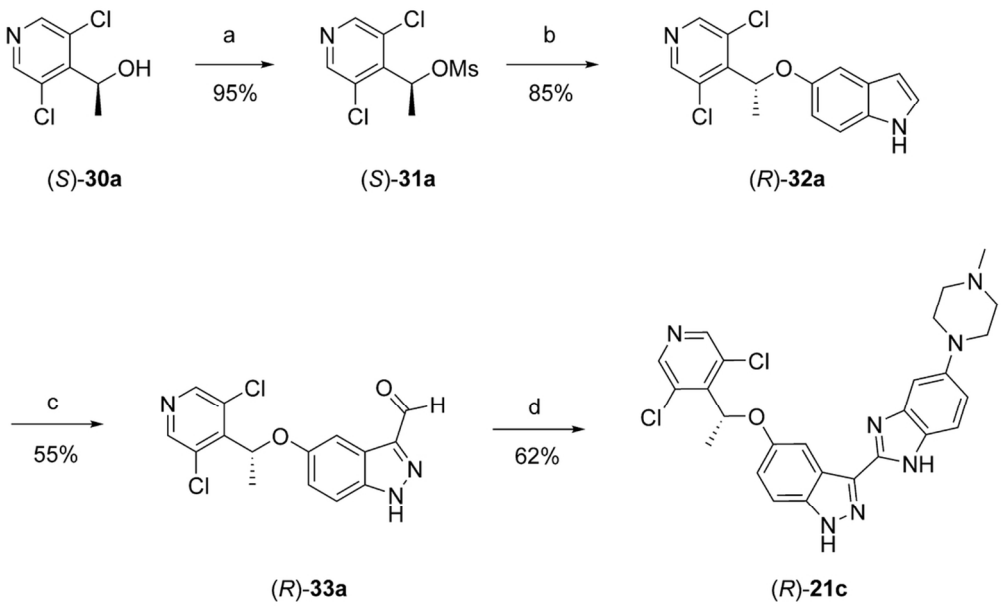

Scheme 6[a] [a]Reagents and conditions: (a) MsCl, Et_3N, CH_2Cl_2, 0 °C to rt; (b) 5-hydroxyindole, Cs_2CO_3, DMF, 70 °C; (c) $NaNO_2$, HCl, H_2O/dioxane, 0 °C to rt; (d) (i) **40c**, H_2, 10% Pd/C, MeOH, rt; (ii) S_8, DMF, 90 °C.
50x30mm (600 x 600 DPI)

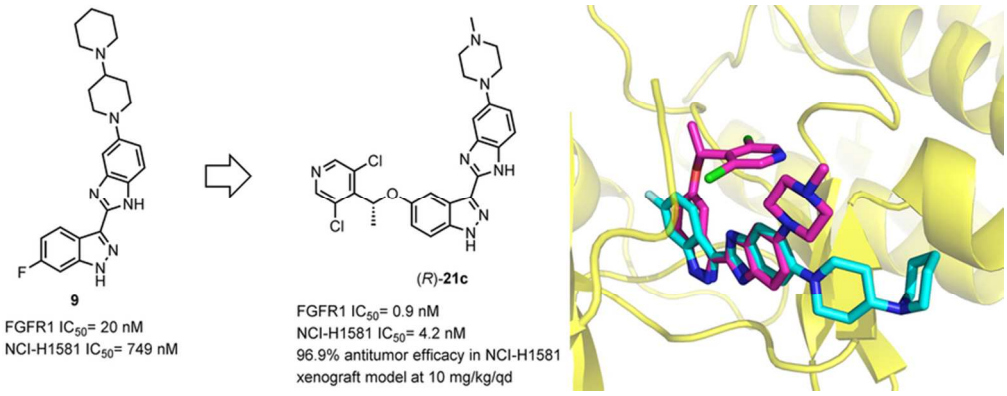

Table of contents graphic
76x29mm (300 x 300 DPI)